

# UC San Diego

## UC San Diego Electronic Theses and Dissertations

### Title

Controllability of Magnetic Nanocarriers for Targeted Drug Delivery

### Permalink

<https://escholarship.org/uc/item/7sq8g2ww>

### Author

Kandah, Udai

### Publication Date

2022

Peer reviewed|Thesis/dissertation

UNIVERSITY OF CALIFORNIA SAN DIEGO

Controllability of Magnetic Nanocarriers for Targeted Drug Delivery

A Thesis submitted in partial satisfaction of the requirements  
for the Master of Science

in

Engineering Sciences (Mechanical Engineering)

by

Udai Kandah

Committee in charge:

Professor Ratnesh Lal, Chair  
Professor Javier Garay  
Professor KeiKo Nomura

2022

Copyright

Udai Kandah, 2022

All rights reserved.

The Thesis of Udai Kandah is approved, and it is acceptable in quality and form for publication on microfilm and electronically.

University of California San Diego

2022

## TABLE OF CONTENTS

THESIS APPROVAL PAGE .....	iii
TABLE OF CONTENTS.....	iv
LIST OF FIGURES .....	v
LIST OF TABLES .....	viii
VITA.....	ix
ABSTRACT OF THE THESIS .....	x
INTRODUCTION.....	1
CHAPTER 1 .....	9
CHAPTER 2 .....	28
CHAPTER 3.....	40
CONCLUSION .....	60
REFERENCES.....	63

## LIST OF FIGURES

Figure 1: Shows blood-brain barrier (BBB) as a blocking path to the central nervous system (CNS) vessels (reproduced with permission from [59])..... 3

Figure 2: shows the magnetic dipole of different magnetization types..... 13

Figure 3: increase the number of magnetic nanoparticles results in a significant increase in the magnetization ..... 15

Figure 4: Flow inside the channel of the microfluidic chip..... 17

Figure 5: velocity vs distance profile for the 3 flow rates A)  $Q = 2\text{ul/min}$  and average velocity of  $0.833\text{mm/sec}$  B)  $Q = 10\text{ul/min}$  and average velocity of  $4.165\text{mm/sec}$  C)  $Q = 20\text{ul/min}$  and average velocity of  $8.329\text{mm/sec}$ ..... 19

Figure 6: A) shows the magnetic field vectors of the magnet B) shows the magnetic force applied on the nanobowls with the direction..... 22

Figure 7: drag force vs distance along the x-direction of the microfluidic chip for nanobowls suspended in water at 3 different flow rates A)  $Q = 2\text{ul/min}$  B)  $Q = 10\text{ul/min}$  C)  $Q = 20\text{ul/min}$ ..... 24

Figure 8: drag force vs distance along the x-direction of the microfluidic chip for nanobowls suspended in 22% glycerin-Water Solution at 3 different flow rates A)  $Q = 2\text{ul/min}$  B)  $Q = 10\text{ul/min}$  C)  $Q = 20\text{ul/min}$ ..... 25

Figure 9: a non-detailed steps of having magnetic nanobowls..... 33

Figure 10: A) shape of the microfluidic chip. B) dimensions of the channel. C) system of the microfluidic chip with the magnet and syringe pump ..... 39

Figure 11: A) TEOS collides with polystyrene to form a silica nanoparticles with polystyrene inside. B) SEM image of silica spheres with polystyrene inside C) TEM image of silica spheres with polystyrene inside ..... 41

Figure 12: An amino silane ((3-Aminopropyl)triethoxysilane is attached to the silica sphere to modify the surface for carboxylate iron oxide attachment ..... 42

Figure 13: Activation of carboxylate iron oxide using EDC..... 43

Figure 14: A) diagram shows attachment of carboxylate iron oxide to silica spheres with PS  
 B) SEM image of attached iron oxide to silica spheres C) TEM image of attached iron oxide to silica spheres..... 44

Figure 15: A) schematic shows the DMF dissolves only the PS form the silica nanospheres and produces nanobowls B) SEM image of nanobowls with carboxylate iron oxide C) TEM of nanobowls without iron oxide attached to better see the cavities..... 45

Figure 16: A) SEM image of silica nanospheres with non-activated iron oxide. B) SEM image of silica nanospheres with activated iron oxide. C) EDS data shows the compounds in non-activated iron oxide sample. D) EDS data shows the compounds in activated iron oxide sample. E) Iron concentration of each sample from the EDS data. .... 46

Figure 17: A) a schematic of the surface charge in green shows the silica sphere with negative charge coated with AEAPTMS positive charge and the carboxylate iron oxide with negative charge. B) The actual average reading of 5 different sample on zeta potential ..... 47

Figure 18: A&B) SEM image shows the size of the nanobowls C) Size distribution of nanobowls after 2 hours and 1 week D) size distribution of nanobowls without iron oxide E) size distribution of nanobowls with iron oxide..... 49

Figure 19: Flow profile inside a microfluidic channel ..... 50

Figure 20: A) magnetic nanobowls dispersed in water B) magnetic nanobowls getting attached using a 0.4T magnet with pulling force of 18.71 lbs. C) nanobowls a moved

to the magnet side D) shows the distance where the nanobowls start getting attracted  
after the presence of different magnet size and pulling force .....51

Figure 21: Nanobowls solvent is injected to the microfluidic chip with a magnet to one side 53

Figure 22: A) absorption measurement for different flowrates and concentration B) plot of  
absorption with concentration ..... 55

Figure 23 A) drawing of the microfluidic chip mold. B) nanobowls suspended in water passed  
through the microfluidic chip and collected at the four outlets. C) nanobowls  
suspended glycerin-water passed through the microfluidic ..... 58



LIST OF TABLES

Table 1: Absorption of a reduced concentration of iron oxide nanobowls (IONBs) suspended  
in water at 3 different flow rates..... 54

Table 2: Absorption of a reduced concentration of iron oxide nanobowls (IONBs) suspended  
in glycerin-water at 3 different flow rates. .... 56

## VITA

2021 Bachelor of Science in Mechanical Engineering, University of California San Diego

2022 Master of Science in Engineering Sciences (Mechanical Engineering), University of California San Diego

## ABSTRACT OF THE THESIS

Controllability of Magnetic Nanocarriers for Targeted Drug Delivery

by

Udai Kandah

Master of Science in Engineering Sciences (Mechanical Engineering)

University of California San Diego, 2022

Professor Ratnesh Lal, Chair

Nanobowls is a modified structure of nanoparticles that holds drug inside for therapeutics and diagnosis. However, drug delivery in nanocarriers have a lot of limitations that effect its efficiency due to location of the diseases and ability of controlling the nanocarriers. A potential solution is to make the nanocarriers magnetic to be able to guide them to the targeted region where the drug is going to be released. For this, we designed a stable nanobowls made from Silica ( $\text{SiO}_2$ ) that can encapsulate the drug inside a cavity. The nanobowls were magnetized using iron oxide to enable responsivity to a magnetic field. A

scanning electron microscopy (SEM) and transmission electron microscopy (TEM) images was captured to confirm the structure of the magnetized nanobowls and dynamic light scattering (DLS) to test aggregation. A mathematical analysis was performed on the flow and the magnetized nanobowls for a force balance between magnetic force and drag force. Guiding efficiency was examined in vitro using a Y shape microfluidic chip system has square cross section area and width of 200 $\mu$ m. A N42 magnet with a surface field of 0.42 T in and a pulling force of 27.83 lbs was used to guide the magnetic nanobowls. An absorption test was performed on the nanobowls passed through the microfluidic chip system and the concentration was found. As expected, the concentration of the nanobowls decreases in more viscous solvents and with increasing the flow rate and distance from the nanobowls. Further work is required to use multiple magnets to increase responsibility.

## INTRODUCTION

### **What are nanoparticles and nanobowls**

Nanoparticles are used in many applications such as cancer therapy, diagnostic testing, HIV/AIDS treatment, and Nutraceutical delivery [2]. An example of nanoparticles are Janus particles which are colloidal particles with two or more unique surface chemistries [1]. There are many reasons for using nanoparticles over other drug delivery systems. Nanoparticles can be driven using magnetic field to the diseased location which means more drugs going to be delivered to the targeted tumor and at the same time fewer side effects will happen [3]. Also, they can be controlled for an on-demand drug release [4]. However, with all these pros for nanoparticles there are some cons such as, nanoparticles could be toxic this depends on the chemicals the nanoparticles are made from [3], also the drugs that are encapsulated inside the nanoparticles could leak out through the delivery process to the tumor.

Nanobowls are nanoparticles with a single hole (cavity) on the surface. This hole allows the drug to be stored inside of the nanobowls so that they are more protected and more stable than storing it inside a lipid bilayer that surrounds the nanoparticle. The inside of the nanobowls can be made either hydrophobic or hydrophilic depending on the type of the drug that is going to be loaded [5]. The purpose of the nanobowls is to act as a shuttle to carries the drug to a certain location in the body [6].

### **Nanoparticles in therapeutic uses**

Nanotechnology is nowadays widely used in treating many different diseases and solving many problems that were previously difficult [7]. This has proved that nanoparticles with therapeutic payloads are very strong candidates for drug delivery treatment. However, magnetic nanoparticles have improved the nanoparticles functionality by being able to control them for

drug delivery and diagnostics such as magnetic resonance imaging (MRI) [8]. It was also proven that magnetic nanoparticles are nontoxic and biodegradable [45] [46]. This means that they will not harm other body organs and they will degrade and vanish by themselves after a period of time. One of the most important uses of nanoparticles is in treating brain diseases (dementia). In Professor Lal's lab. We worked on nanobowls that can be loaded with different kinds of drugs such as Ketamine which is used for depression treatment as it manipulates a neurotransmitter called glutamate which is what makes most of the neurons in the brain to communicate with each other and without it, the brain is not functional [9]. And Anle138b which is used for the treatment of Alzheimer and recrudesces the progression and prion and Parkinson's disease in animal models which are caused by an abnormal aggregation in protein so called amyloid [10]. As anle138b modulate the  $\alpha$ -synthesis and prevents neurodegeneration in mouse models [11].

However, some drugs are difficult to load into the nanobowls and that is because of the properties of the drug which causes some limitations such as where the drug is going to be loaded (in a lipid bilayer or inside the nanoparticles). And preparing the right environment for the drug could be a challenge as some drugs are lipophilic or hydrophilic and other are both lipophilic and hydrophilic. However, if the drug is both hydrophobic and hydrophilic such as Ketamine, it will leak out of from the nanobowls.

Nanobowls will help move the drug to the tumor location and can also be controlled for on demand release. This is very important so that the drug will directly attack the tumor with higher concentration and less time is required to get to the tumor. The nanoparticles can be controlled in the blood vessels using an external magnetic field that will attract the iron oxide ions attached to the nanobowls. And it can be controlled for an on-demand drug release as the nanobowls can be covered by a thin layer such as NIPAM, which is temperature and PH

sensitive [13] [12] whereas the drug is being held inside the cavity. By changing the temperature or the PH, the NIPAM layer becomes unstable and allows the drug to come out of the nanobowls.

### Magnetic nanobowls for dementia treatment

To access the brain, the magnetic nanobowls have to go through a vessels central nervous system (CNS). However, the CNS has a limited permeability represented by a path block which is known as blood-brain barrier (BBB) that surrounds most of the blood vessels in the brain [14]. The BBB allows only certain particles to pass through such as water, oxygen and lipid soluble substances [15].

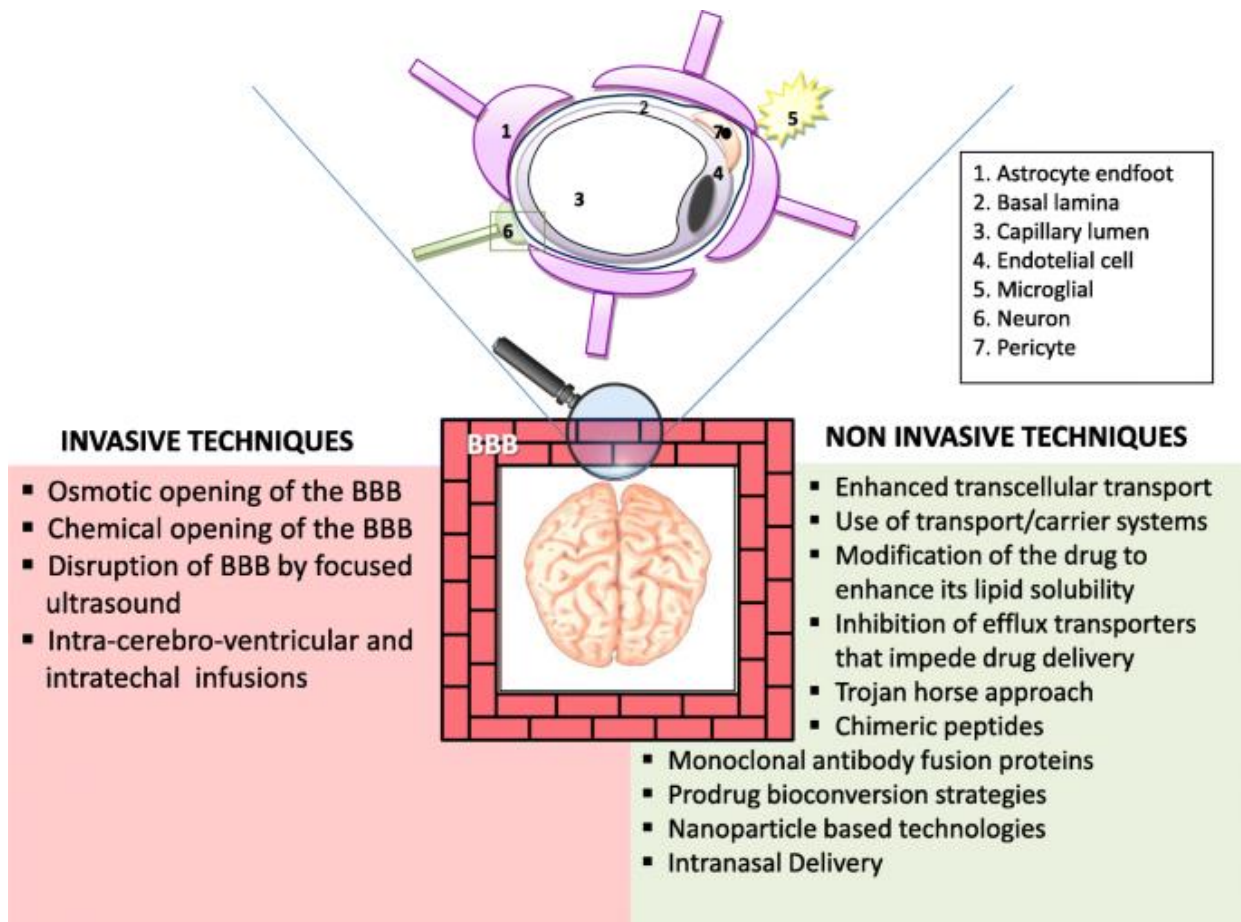


Figure 1: Shows blood-brain barrier (BBB) as a blocking path to the central nervous system (CNS) vessels (reproduced with permission from [59])

This results in an obstacle that prevents the nanobowls and drugs from reaching the tumor inside the brain. Many methods were developed to overcome the BBB obstacles. However, depending on the drug that is going to be delivered, the right method to pass the BBB should be chosen wisely. Some of these methods are [16]:

1. Modifying the drug to be more lipid soluble
2. Monoclonal antibody fusion proteins
3. BBB Transient disruption to force the drug in
4. Different routes to the brain
5. Pull the magnetic nanobowls using a magnetic field

As described before, since BBB allows lipid soluble substances to pass. Then by the first method, the drug can be made more lipid soluble by adding lipid groups to the polar end of it [16]. The second method involves modifying the drug as an IgG fusion protein, this IgG helps in binding the endogenous BBB receptors such that it makes the penetration easier [16]. In the third method, different techniques were used to break the tight junction in the BBB, such as ultrasounds and noxious agents. However, this method causes a lot of side effects because it allows many other unwanted substances to pass through the BBB [17][18]. The fourth method was proved to be very successful, however not all parts of the brain are accessible by different routes [18]. Last but not least, using magnetic nanobowls with the drug is being held inside the nanobowls can be pulled through the BBB which leaves the blood vessels intact [21]. It was proved in previous studies that the concentration of magnetic particles in the brain increased by a huge factor when a magnetic field was exerted, as compared to without a magnetic field. Although, it's important to take into account the size of the magnetic nanobowls as until now, it



was proved that particles with size over 150nm still cannot pass through the BBB even with magnetic force.

### **Benefits of using magnetic nanobowls in drug delivery**

Drug delivery methods other than magnetic nanobowls have a lot of limitations that could cause side effects and harm other body organs. For example, Intravenous (IV) therapy or pills can deliver drug to the body, however using these methods will take time for the drug to get to the diseased region and react. also, the patients generally require high doses of the drug in order to reach the diseased region, yet only a small percentage reaches to the area of the disease. Whereas the rest of the drug would flow to other body organs and results in detrimental side effects. Moreover, for some diseases the drug will keep a rapid clearance from the diseased region, for example as it was described before in the brain diseases the BBB will not allow the nanoparticles to be closer than 40-50 cm from the diseased region [21]. This leads to not having enough concentration of the drug to perform an effective therapeutic impact. These limitations increase the cost, toxicity and the efficiency of drug delivery in treatment [19].

The benefit of using magnetic nanoparticles here is that they can be guided by a magnetic field to the disease region. Almost 40% of the magnetic nanoparticles are internalized by the liver in the first 30 minutes from administration and almost 80 % after 1 hour [20] [21]. However, if those nanoparticles are magnetized then we can drive them using a magnetic field through a different path in the blood stream or bypass through the liver without being internalized.

For the nanobowls prototype, the intuition is that these nanobowls can be magnetized using iron oxide and driven through the blood stream where they can release the drug. Using this method, two problems can be solved, where the patient does not need to take more doses than

what is required and the other one is that the concentration of drug at the diseased region will be higher. Also, the drug released from the nanobowls can be released based on the PH and temperature of the disease region, this means that the nanobowls can be loaded with a high number of doses than what the disease requires and release some ratio at a time, this will save a lot of time since it's not required waste time getting to the disease region every time. Moreover, nanoparticles allow the drug to cross the BBB and that is by using the trafficking mechanism without leaving any damage to its integrity [21].

Magnetic nanobowls are very powerful as they can get to the diseased region in only 5 minutes after injection. They are also very stable as they reach a steady state in 30-120 minutes post-injection [21] [22]. After a certain time, the magnetic nanobowls diminish away by themselves from body circulation by either the liver or the spleen [22].

### **Controlling using a magnetic field**

Magnetic nanobowls are affected by multiple factors in magnetic control such as size, shape, flexibility, coating, magnetic coating and drug loading [23]. This means the design of the magnetic nanobowls has to be specific for clinical needs. To be able to control the magnetic nanoparticles through the blood, the magnetic field has to overcome the blood drag force and yield forces. To achieve this, the magnetic moment applied to the nanoparticles need to be maximized which could be done in different ways:

1. Increase the volume of nanoparticles
2. Make the magnetic carrier superparamagnetic
3. Increasing the iron oxide particles on the nanobowls surface and distribute them more uniformly
4. The magnet should provide a strong uniform magnetic field

It has been proven that increasing the volume is directly proportional to the magnetic moment applied on the nanoparticles by increasing the saturation point. On the other hand, increasing the volume would result in many obstacles that will negatively affect the delivery system [25]. Some of these obstacles are not being able to cross the BBB. Not only that, increasing the volume would also causes a problem with going through small blood vessels such as capillaries. Also, an important issue with increasing the volume is that the particles are not able to reach a superparamagnetic regime where the particles have the highest magnetization and responsibility to magnetic field.

Usually, the iron oxide particles attached to the nanobowls have random poles directions that makes them cancel each other's magnetic moments to reduce aggregation. However, once a magnetic field is applied, the poles align in one direction which is the direction of the magnetic field to reach a superparamagnetic regime. This can increase the magnetic moment by almost 15-fold [26] [27]. However there are a lot of limitations that can prevent the iron oxide particles from reaching this regime. This limitation will be discussed later in chapter 1.

Increasing the concentration of iron oxide particles or the strength of the magnet used will increase the attraction forces by increasing the magnetic moment applied on the magnetic particles. However, an important factor that needs to be taken into consideration here is that increasing the magnetic particles make the nanobowls more toxic, which could leads of a lot of side effects such as metal fume fever [28]. Also, getting exposed constantly to a magnetic field will harm many parts of the body.

### **Microfluidic chip for nanobowls control**

Microfluidic chips can be used for [29]:

- Nanoparticles separation

- Detection/deionization
- Cell sorting
- Protein analyzation
- Mixing
- Transport

In this Thesis, microfluidic chips were used to separate the magnetic nanobowls from the solvent using a magnetic field. The microfluidic chip was made out of 3 separate channels a parent and 2 daughters that are combined in a Y shape. A magnet of 0.4 Tesla was used on one side of the microfluidic chip and the nanobowls with the solvent enters from the parent channel. Then using the magnet, we separate the magnetic nanobowls to one side of the daughter channels and the other side of the daughter channel with remain with the solvent as shown in figure 10.

This is an important test for our study as it helps to determine if we are going to be able to control the magnetic nanobowls through the blood vessels. However, this test doesn't represent the control in deep tissues as the magnetic force fall quickly with distance [30] [31].

## CHAPTER 1

### Theoretical calculations

#### 1.1 Stability of particles

Colloidal stability is to ensure the particles remain dispersed in the organic solvent and that there is no aggregation present. This means that the energy between the particles resulting from attractive forces should be less than the Boltzmann constant ( $K_B$ ) multiplied by the absolute temperature (T) - which means the sedimentation rule must hold. Also, particles in the organic solvent tends to collide and cluster due to attractive forces such as van der Waals forces which result in aggregation. To make the particles more stable they should be covered with a dispersant layer where these particles can absorb which was Polyethylene glycol (PEG) for our nanoparticles [32].

##### 1.1.1 Sedimentation

Gravity causes the particles suspended in a solvent to precipitate at the bottom of reservoir. However, sedimentation ensures that the particles are suspended in the solvent by showing the gravitational sedimentation energy ( $E_s$ ) has a greater value than the thermal energy ( $E_t$ ). To find the  $E_s$  we can use following equation

$$E_s = \Delta\rho gVh \quad \text{Eq (1)}$$

Where  $\Delta\rho$  is the density difference, g is gravity, V is the volume of the particle and h is the height of settling. Using density of silica particles in water of  $2000 \text{ kg/m}^3$  a radius of 150nm and assuming it's a sphere, gravity of  $9.81 \text{ m/s}^2$  and a setting height of 1.5 cm which was a 1ml of water the gravitation sedimentation energy was calculated to be  $4.16 \times 10^{-18} \text{ J}$ . On the other hand, the thermal energy can be calculated as follows

$$E_t = K_b T \quad \text{Eq (2)}$$

Where  $K_b$  is the Boltzmann constant is equal to  $1.38 \times 10^{-23}$  J/K and T is the absolute room temperature in kelvin which is 293 K. The thermal energy was calculated to be  $4.04 \times 10^{-21}$  J. We see here that the gravitational sedimentation energy is 3 orders higher than the thermal energy which means the particles will not sediment and will remain dispersed in the solvent.

### 1.1.2 Van der Waal's

Van der Waals law states that an attractive force could present between 2 neighbors' particles due to the electric polarization on the particles that could cause a permanent dipole. This force mainly depends on the size of the particles and the distance between them as they present in the solvent.

$$F_{vw}(r) = -\frac{AR_1R_2}{6(R_1+R_2)r^2} \quad \text{Eq (3)}$$

Where  $F_{vw}$  is the van der Waals force, A is the Hamaker constant which has a value of  $8.53 \times 10^{-21}$  J for silica particles in water,  $R_1$  and  $R_2$  are the spherical bodies radii of the particles and r is the distance between the 2 particles surfaces. The negative sign indicates that the van der Waals force is an attractive force.

### 1.1.3 Concentration of particles

Increasing the concentration of particles for the same volume of solvent causes the particles to aggregate. Sonication could help in reducing this aggregation, however if the concentration is too heigh that will not allow the particles to disperse in the solvent homogenously. To calculate the number silica particles in a solvent we need to find the molar weight of silica ( $\text{SiO}_2$ ) which is 60.08 g/mol. From measuring the yield after drying the silica nanoparticles in a glass vial the average mass of 20 trials was 1.09 mg. From here, the moles of silica particles per liter of water is found as follows

$$M = \frac{m \cdot \text{mass}}{V} \quad \text{Eq (4)}$$

Where M is the molarity (moles per liter), m is the molar weight and V is the volume of the solvent which was 700 uL of water. The molarity was then calculated to be  $2.60 \times 10^{-2}$  mol/L. And the particles concentration which is the number of silica particles can be calculated as follows

$$n = N_A M \quad \text{Eq (5)}$$

Where n is the number of particles and  $N_A$  is Avogadro's number which is equal to  $6.02 \times 10^{23}$ . The number of particles was then calculated to be  $1.56 \times 10^{22}$ . We see that we have a huge amount of magnetic nanobowls inputted into the body. This means that even if the cavity where the drug is being held in the nanobowls is not big enough we can still transfer a good amount of drug. It's also important to keep in mind that if a huge amount of particles was inputted into the body that might increase the toxicity.

## 1.2 Magnetization

Magnetization type controls the magnetic moment applied on the magnetic nanobowls with make them either more or less responsive to a magnetic field. Magnetization describes the direction of the pole in the magnetic particles which expresses the density of the induced dipole moments. Aligning the direction of the poles in the same direction would allow to increase the magnetic responsivity by reducing the cancelation of magnetic moment applied by a magnet on a magnetic nanobowls.

### 1.2.1 Magnetization types

In The absence of external magnetic field, there are 3 types of how the magnetic moment of the atoms is oriented the first one is that there is no magnetic moment dipole which means the material is no responsive to a magnetic field. The second one is the magnetic moment is aligned

in a certain direction either in the same direction or in two opposite directions as shown in figure

2. The last one is magnetic moment of atoms is oriented randomly in the material and the net dipole moment in the material is equal to zero. However, material can be magnetized by



magnetic field and temperature into 6 types of magnetizations which are:


1. Diamagnetic: where the material is magnetized in the opposite direction ( $180^\circ$  out of phase) of the magnetic field. And the material doesn't retain its magnetic properties when the magnetic field is removed.
2. Paramagnetic: the material is magnetized in the same direction as the magnetic field under a high magnetic field intensity or a low absolute temperature to form a weak attracting. All the dipole in the material will be parametrized at the saturation of magnetization point.
3. Ferrimagnetic: is a material that has some atoms with opposing dipole magnetic direction and different magnetic moment magnitude without any magnetic field applied. The different magnitude of magnetic moment allows the material to be strongly attracted to a magnetic field.
4. Antiferromagnetic: it's the same as Ferrimagnetic however all the atoms have the same magnetic moment magnitude which makes the magnetic moment of the atoms cancel each other and reduces the material attraction to a magnetic field.
5. Ferromagnetic: is a material where the magnetization of the atoms is all aligned in the same direction with the same magnetic moment magnitude. This type is associated with iron, cobalt and nickel which gives them a very strong attraction response to a magnetic field.



6. Superparamagnetic: it's a special case of ferromagnetic and ferromagnetic particles.

However, it also hold some paramagnetic properties such as the poles are only aligned in the same direction if the magnetic field exist.

Magnetization type	Pericles dipole direction	
	Without magnetic field	With magnetic field
Diamagnetic	No magnetic dipole	↓ ↓ ↓ ↓ ↓ ↓ ↓ ↓ ↓ ↓
Paramagnetic		↑ ↑ ↑ ↑ ↑ ↑ ↑ ↑ ↑ ↑
Ferromagnetic	↑ ↑ ↑ ↑ ↑ ↑ ↑ ↑ ↑ ↑	↑ ↑ ↑ ↑ ↑ ↑ ↑ ↑ ↑ ↑
Ferrimagnetic	↑ ↓ ↑ ↓ ↑ ↓ ↑ ↓ ↑ ↓	↑ ↓ ↑ ↓ ↑ ↓ ↑ ↓ ↑ ↓
Antiferromagnetic	↑ ↓ ↑ ↓ ↑ ↓ ↑ ↓ ↑ ↓	↑ ↓ ↑ ↓ ↑ ↓ ↑ ↓ ↑ ↓
superparamagnetic		↑ ↑ ↑ ↑ ↑ ↑ ↑ ↑ ↑ ↑



Magnetic Filed Direction

Figure 2: shows the magnetic dipole of different magnetization types

### 1.2.2 Superparamagnetic

Superparamagnetic type is very useful in applications such as drug delivery and MRI. This is because as the magnetic field is removed the particles do not experience any magnetic properties, meaning that the dipole of the particles is randomly aligned. Therefore, there are no attraction forces between the particles which eliminate the driving force for aggregation this is why superparamagnetic particles are more preferable than ferri- and ferro-magnetic particles. Also, superparamagnetic particles have a higher saturation point comparing to paramagnetic

particles. Meaning that they can have a higher magnetization moment and as result more responsive to a magnetic field.

However, to achieve a superparamagnetic there are some requirements such as the temperature and the size of the particles. For ferri- and ferro-magnetic materials to become superparamagnetic then they must approach what is called block temperature. This this temperature point can be found experimentally by finding the intersection point between the zero-field cooled (ZFC) and field-cooled (FC) or theoretically using the following equation [33]

$$T_B = \frac{KV}{25K_b} = \frac{4\pi K r_o^3}{75K_b} \quad Eq(6)$$

Where  $T_B$  is the blocking temperature  $K$  is the anisotropy constant which is equal to  $1.1 \times 10^4 \text{ J/m}^3$  for iron oxide [34],  $V$  is the volume of the iron oxide which has a radius of  $15 \pm 2$  nm and  $K_b$  is Boltzmann constant that is equal to  $1.38 \times 10^{-23} \text{ J/K}$ . and  $T_B$  was calculated to be 293.4K which is room temperature. This only works for particles with very small size and by increasing the particles size then achieving superparamagnetic regime becomes impossible. This radius can be calculated using the following equation [33]

$$r_o = \left( \frac{6K_b T_B}{K} \right)^{\frac{1}{3}} \quad Eq(7)$$

Where is the transition position radius from superparamagnetic to single-domain regime.  $K_b$  is Boltzmann constant that is equal to  $1.38 \times 10^{-23} \text{ J/K}$ ,  $T_B$  is the blocking temperature and  $K$  is the anisotropy constant. For Iron oxide with a value of  $K$  equal to  $1.1 \times 10^4 \text{ J/m}^3$  and at a room temperature then  $r_o$  was calculated to be 13nm.

It can be recognized that it's not possible to increase the size of the magnetic nanoparticles to stay in the superparamagnetic regime. However, to increase the magneticity it is possible to increase the number of magnetic nanoparticles attached to the nanobowl this was

found to be a very effective way to increase the responsivity as increasing the number of iron oxide particles attached to the nanobowls just by a small factor results in increasing the magnetization by a huge factor.

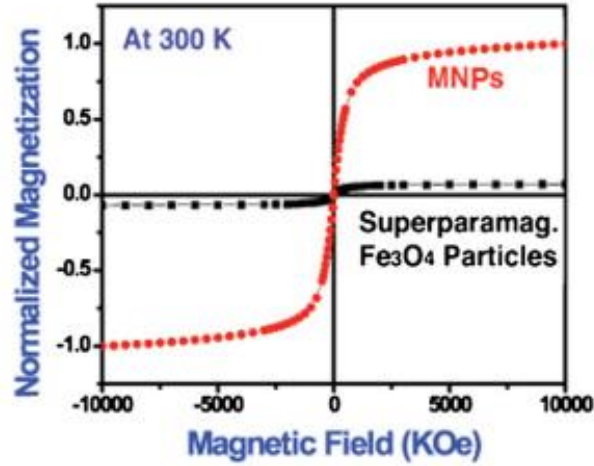


Figure 3: increase the number of magnetic nanoparticles results in a significant increase in the magnetization

### 1.2.3 Relaxation Time

There are 2 types of relaxations that explains the alignment of the particles in the direction of the magnetic field which are Nèel relaxation and Brownian relaxation. Nèel relaxation theory is providing enough energy to align the particles spins in the direction of the external magnetic field by overcoming the anisotropy energy barrier This theory is usually applied to particles with the size of 20 nm or less. Nèel relaxation can be calculated the following equation [35]

$$\tau_N = \tau_0 e^{\left(\frac{KV}{k_b T}\right)} \quad Eq(8)$$

Where KV is the height of the energy barrier where K is the density of magnetic anisotropy energy and V is the volume.  $k_b$  is Boltzmann constant and T is the temperature.

However, Brownian relaxation theory is the process of rotation the whole particle in the direction

of the external magnetic field, and it's usually applied to particles of the 20 nm or greater.

Boltzmann constant can be calculated using the following equation [36]

$$\tau_B = \frac{3V_h\eta}{K_bT} \quad Eq(9)$$

Where  $V_h$  is the hydrodynamic volume,  $\eta$  is the viscosity of the solvent,  $K_b$  Boltzmann constant and  $T$  is the temperature. For large particles it's faster for the particles to align the dipole direction by rotating the whole particles. On the other hand, for small ones it's faster to orient the spins. For our case since we are using iron oxide particles with an average size of 15nm we will only have Néel relaxation.

### **1.3 Flow Characterization in microfluidic chip**

A targeting test of the magnetic nanobowls has been done inside a microfluidic chip. This system was used to attract the nanobowls using a magnetic field through a small channel that represents the vessels in the human body at different flow rates and speeds. This test will help recognizing the effectivity and the ability to control the nanobowls through the body.

#### **1.3.1 Velocity flow profile**

Navier-Stokes equation can be used to find the flow shape. The flow in channel was assumed to be incompressible meaning the mass of fluid going in is the same as the mass going out [56]. Fully developed meaning the flow has a parabolic flow profile. No slip boundary condition meaning the velocity at the wall equals to zero. Steady flow meaning flow is consistent and does not change with time. Finally, the flow is along the x-axis [57].

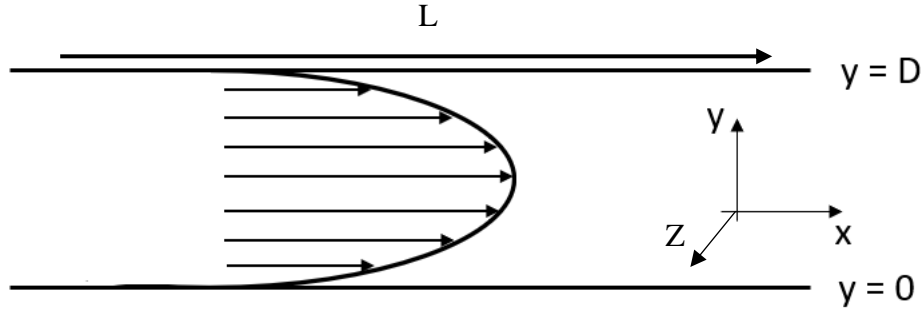


Figure 4: Flow inside the channel of the microfluidic chip

Starting from the conservation of momentum In Navier-Stokes theorem the velocity profile can be found as follows.

$$\rho \left( \frac{\partial u}{\partial t} + \frac{u \partial u}{\partial x} + \frac{v \partial u}{\partial y} + \frac{w \partial u}{\partial z} \right) = -\frac{\partial P}{\partial x} + \mu \left( \frac{\partial^2 u}{\partial x^2} + \frac{\partial^2 u}{\partial y^2} + \frac{\partial^2 u}{\partial z^2} \right) \quad Eq(10)$$

Where  $\rho$  is density of the fluid,  $v$  is velocity along the  $y$ -direction,  $P$  is pressure and  $\mu$  is dynamic viscosity. Because the flow was assumed to be fully developed and if we assume it's only a 2D flow then  $\frac{\partial u}{\partial x}$ ,  $\frac{\partial^2 u}{\partial x^2}$  and  $\frac{\partial^2 u}{\partial z^2}$  are equal to zero. And since the flow was assumed to be only in the  $x$  direction then  $v$  and  $w$  are equal to zero. Also, since the flow is steady then  $\frac{\partial u}{\partial t}$  is equal to zero. The equation becomes.

$$\frac{\partial^2 u}{\partial y^2} = \frac{1}{\mu} \frac{\partial P}{\partial x} \quad Eq(11)$$

Integrating twice with respect to  $y$  we get

$$u = \frac{1}{\mu} \frac{\partial P}{\partial x} \frac{y^2}{2} + c_1 y + c_2 \quad Eq(12)$$

Where  $c_1$  and  $c_2$  are constants. Using the boundary condition which are  $u = 0$  at  $y = 0$  and  $u = 0$  at  $y = D$  then we can solve for the constants.

$$c_2 = 0 \quad Eq(13)$$

$$c_1 = -\frac{1}{\mu} \frac{\partial P}{\partial x} \frac{D}{2} \quad Eq(14)$$

Now the constants can be substituted into the velocity to find the velocity profile equation.

$$u = -\frac{1}{2\mu} \frac{\partial P}{\partial x} (y^2 - Dy) \quad Eq(15)$$

Notice that the velocity equation confirms that the flow should be parabolic since we have a second order equation. However, note here that to solve for the velocity profile at different points we need the pressure gradient. But since in our experiment the known was the flow rate then we can solve the pressure gradient in terms of the flow rate as follows.

$$Q = \int u dA \quad Eq(16)$$

Where Q is the flow rate and A is the area. The cross-section area is given by multiplying the y distance which starts at 0 and ends at D by the z distance which also starts at zero and ends at D as given in figure 4 above. By substituting u and into the equation and solve the integration we get the following.

$$Q = -\frac{1}{2\mu} \frac{\partial P}{\partial x} \int_0^D \int_0^D (y^2 - Dy) dy dz \quad Eq(17)$$

$$Q = \frac{D^4}{12\mu} \left( \frac{\partial P}{\partial x} \right) \quad Eq(18)$$

Solving for  $\frac{\partial P}{\partial x}$  and substituting in the velocity profile equation founded in equation 15.

We get the following.

$$u = \left( -\frac{6Q}{D^4} \right) (y^2 - Dy) \quad Eq(19)$$

This equation can be used to find the velocity along the y axis at any location along the microfluidic chip.

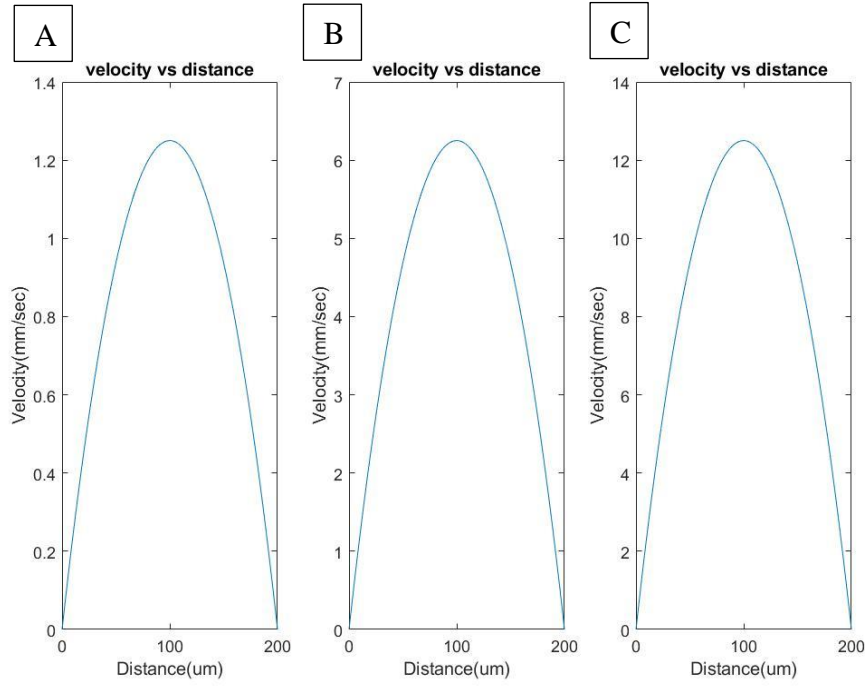


Figure 5: velocity vs distance profile for the 3 flow rates A)  $Q = 2\text{ul/min}$  and average velocity of  $0.833\text{mm/sec}$  B)  $Q = 10\text{ul/min}$  and average velocity of  $4.165\text{mm/sec}$  C)  $Q = 20\text{ul/min}$  and average velocity of  $8.329\text{mm/sec}$

It's important to note that the velocity here was found for a 2D case. In a 3D case  $\frac{\partial^2 u}{\partial z^2}$  will not equal to zero and Navier-Stokes equation in this case will reduce to the following formula.

$$\frac{\partial^2 u}{\partial y^2} + \frac{\partial^2 u}{\partial z^2} = \frac{1}{\mu} \frac{\partial P}{\partial x} \quad \text{Eq(20)}$$

The partial differential equation here can be solved to get the velocity profile using Saint-Venant method and the boundary condition [62]. If we assume the same boundary conditions as in the 2D model before which are Dirichlet boundary conditions then the velocity will be the following

$$u = -\frac{16\partial P a^2}{\pi^3 \mu \partial x} \sum_{n=1,3,5,\dots}^{+\infty} \frac{1}{n^3} (-1)^{\frac{n-1}{2}} \left[ 1 - \frac{\cosh\left(\frac{n\pi y}{2a}\right)}{\cosh\left(\frac{n\pi b}{2a}\right)} \right] \cos \frac{n\pi z}{2a} \quad \text{Eq(21)}$$

Where a and b here are the cross section dimension of the microfluidic channel where in our case they are both equal to  $200 \mu\text{m}$ .

### 1.3.2 Velocity of flow

The flow was observed to be uniform throughout the microfluidic channel. The average velocity throughout the channel was calculated using the continuity equation which tells that the mass is conserved meaning the mass going into the channel is equal to the mass coming out of the channel. Which can also be referred to as not compressible flow. Thus, the average velocity across the section area of the channel was found using the following equation [49].

$$Q = VA \quad Eq(22)$$

Where Q is the flow rate, V is the velocity and A was the cross-section area which was 0.04 mm<sup>2</sup> and constant throughout the channel. 3 flow rates were used and tested for magnetic controllability which were 2ul/min, 10ul/min and 20ul/min and the velocity was calculated to be 0.833mm/s, 4.165mm/s and 8.330mm/sec respectively.

### 1.3.3 Reynolds number

The micron-scales size of the channel inside the microfluidic chip guarantees that the flow will be fully developed with a no slip conditions and laminar [37] [38]. The main four factors that affects the Reynolds number are fluid velocity, channel diameter, fluid density and fluid viscosity. Reynolds number tells that if the flow will reach a turbulent region or not. The Reynolds number can be calculating as follows:

$$Re = \frac{\rho u L}{\mu} \quad Eq(23)$$

Where Re is Reynolds number,  $\rho$  is density of the flow, L is the characteristic lengths which we will use the diameter here and  $\mu$  is dynamic viscosity of the fluid. The nanobowls were suspended in 2 types of buffers the first one was water with a density of 997kg/m<sup>3</sup> and dynamic viscosity of  $1.002 \times 10^{-3}$  Ns/m<sup>2</sup>. The second is 22% glycerin-Water Solution which has a density of 1052.05kg/m<sup>3</sup> and dynamic viscosity of  $1.767 * 10^{-3}$  Ns/m<sup>2</sup>.



Case 1: water

- 0.833mm/s → Re = 1.66
- 4.165mm/s → Re = 8.29
- 8.330mm/s → Re = 16.58

Case 2: glycerin-Water Solution

- 0.833mm/s → Re = 0.99175
- 4.165mm/s → Re = 4.9587
- 8.330mm/s → Re = 9.9175

As the values for Reynolds number are less than 2000 the flow is proved to be laminar.

This also confirms that all our assumptions for the velocity profile from before are valid.

## 1.4 Forces on the magnetic nanobowls

### 1.4.1 magnetic force

For targeted delivery and to control the magnetic nanoparticles in the channel of the microfluidic chip a magnetic field has been applied by an external a magnet. The magnetic field can be found using the following equation.

$$\mathbf{H} = \frac{\mathbf{B}}{\mu} \quad Eq(24)$$

Where  $\mathbf{H}$  is the magnetic field vector,  $\mathbf{B}$  is the flux vectors which is total magnetic field passing through an area and  $\mu$  is the permeability. The bold letters represent a vector quantity.

The magnetic moment of such a magnet if the inter-particle interaction was neglected can be calculated using the following equation.

$$\mathbf{m} = VM = V\chi\mathbf{H} \quad Eq(25)$$

Where  $m$  is magnetic moment vector,  $V$  is the volume of the spherical iron-oxide particles and  $\chi$  is the difference in magnetic susceptibility between particles and surroundings. The magnetic force acting on the nanobowls and be calculated using the following equation.

$$\mathbf{F}_m = (\mathbf{m} \cdot \nabla)\mathbf{B} \quad \text{Eq(26)}$$

Therefore, since the magnetic field was applied only in the  $y$  directing then force acting on the nanobowls can be found using the following equation

$$\mathbf{F}_{m,y} = \mathbf{m} \frac{dB}{dy} = V\chi\mathbf{H} \frac{dB}{dy} = \frac{4}{3}\pi r^3\chi\mathbf{H} \frac{dH}{dy}\mu \quad \text{Eq(27)}$$

This equation shows that the magnetic force applied on the nanobowls is directly proportional to the radius of the iron-oxide particles attached to the nanobowls. However, it's important to keep in mind that as the radius of the iron-oxide particles increases it becomes impossible to reach superparamagnetic regime.

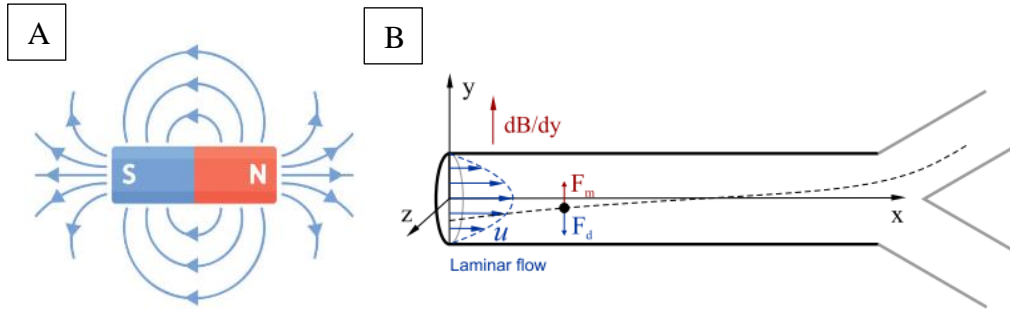


Figure 6: A) shows the magnetic field vectors of the magnet B) shows the magnetic force applied on the nanobowls with the direction

Increasing the radius of the magnetic nanoparticles increases the saturation point which increases the magnetization until it reaches the bulk size. As given in equation 28.

$$M = M_{sb}\left(\frac{r-d}{r}\right)^2 \quad \text{Eq(28)}$$

Where  $M$  is the magnetization of the iron oxide particles,  $M_{sb}$  is the magnetization of the bulk size  $r$  is the radius of the iron oxide particles attached together and  $d$  it the surface thickness.

This shows that there is a limit size where the magnetization can no longer increase.

## 1.4.2 Drag Force

### 1.4.2.1 Drag force on the Flow

The drag force of the flow can be calculated by integrating the shear stress over the area. Since the channel walls are similar the drag force can be calculated for one side and then multiplied by 2 to get the total drag force applied. The following is the derivation for the drag force [58].

$$\tau_w = -\mu \left( \frac{\partial u}{\partial y} \right) \quad Eq(29)$$

Where  $\tau$  is the wall shear stress,  $\mu$  is the dynamic viscosity and  $u$  is the velocity along the  $x$  direction as shown in figure 6 above. Substituting the velocity profile from equation 19 and taking the derivative with respect to  $y$  we get the following.

$$\tau_w = -\mu \left( \frac{\partial \left( -\frac{6Q}{D^4} \right) (y^2 - Dy)}{\partial y} \right) \quad Eq(30)$$

$$\tau_w = \frac{6Q\mu}{D^4} (2y - D) \quad Eq(31)$$

Where  $Q$  is the flow rate and  $D$  is the channel width. By substituting  $y = D$  to find the wall shear stress at the top wall and simplifying we get the following.

$$\tau_w = \frac{6Q\mu}{D^3} \quad Eq(32)$$

This is the shear wall stress only for the upper wall. To find the total wall shear stress we can multiply it by 2 to get the following.

$$\tau_w = \frac{12Q\mu}{D^3} \quad Eq(33)$$

Then the drag force can be calculated by integrating the wall shear stress with respect to the area of the wall. The derivation for the drag force is the following.

$$F_D = \int \tau_w dA \quad Eq(34)$$

$$F_D = \int_0^D \int_0^L \frac{12Q\mu}{D^3} dx dz \quad Eq(35)$$

$$F_D = \frac{12Q\mu L}{D^2} \quad Eq(36)$$

Where  $F_D$  is the drag force and  $L$  is the length of the channel. This equation can be used at any point along the channel to find the drag force.

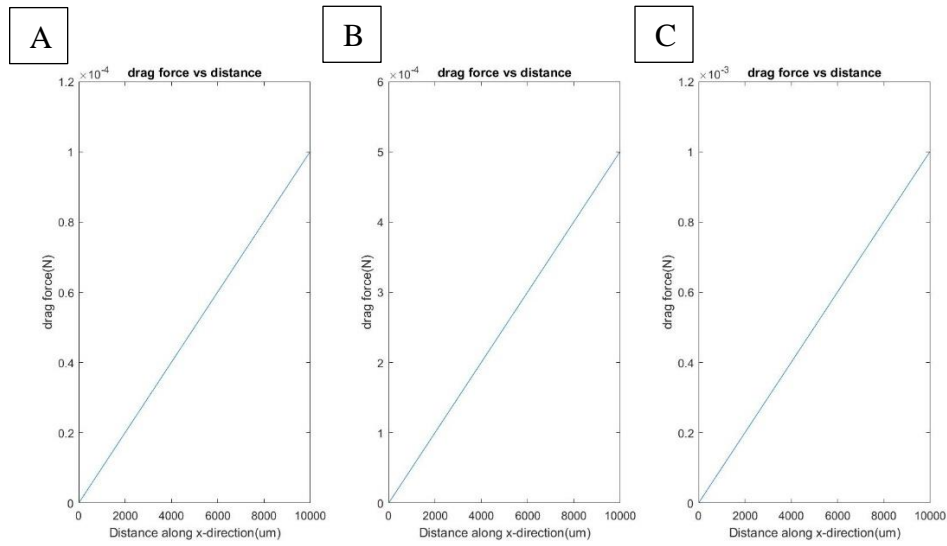


Figure 7: drag force vs distance along the x-direction of the microfluidic chip for nanobowls suspended in water at 3 different flow rates A)  $Q = 2 \text{ ul/min}$  B)  $Q = 10 \text{ ul/min}$  C)  $Q = 20 \text{ ul/min}$

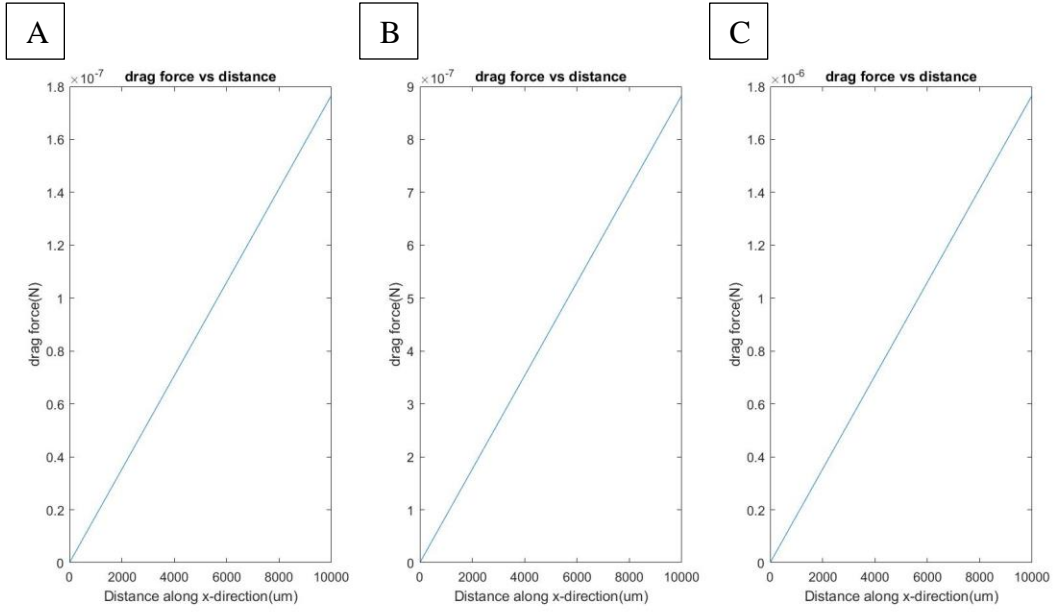


Figure 8: drag force vs distance along the x-direction of the microfluidic chip for nanobowls suspended in 22% glycerin-Water Solution at 3 different flow rates A)  $Q = 2\text{ul/min}$  B)  $Q = 10\text{ul/min}$  C)  $Q = 20\text{ul/min}$

Form equation 36 we see that increasing the fluid dynamic viscosity will increase the drag force. This means nanobowls suspended in water will experience lower drag force compared to those suspended in 22% glycerin-Water Solution. Also increasing the flow rate or the length of the channel will increase the drag force. Lastly increasing the width of the channel will have a huge impact on decreasing the drag force

The shear stress and the drag force here were found only for the 2D case. It will get very complicated in the 3D case that's because the shear stress is a tensor and will have 9 components. Also, the velocity equation used was for the 2D case, whereas if we want to calculate the shear stress and the drag force for the 3D case equation 21 should be used. The following is the tensor of the shear stress.

$$\tau_w = \mu \begin{bmatrix} 0 & \frac{\partial u}{\partial y} & \frac{\partial u}{\partial z} \\ \frac{\partial u}{\partial y} & 0 & 0 \\ \frac{\partial u}{\partial z} & 0 & 0 \end{bmatrix} \quad \text{Eq(37)}$$

### 1.4.2.2 Drag Force on the Nanobowls

The drag force resist the movement of the nanobowls toward the magnetic force applied on the particles. As it will be shown later in the data increasing the drag force on the nanobowls reduces the ability of controlling them to the desired vessel or location. The drag force on the nanobowls can be found using the following equation.

$$\mathbf{F}_{DP} = 6\pi\eta r_p(\mathbf{v}_f - \mathbf{v}_p) \quad \text{Eq(38)}$$

Where  $F_{DP}$  is the drag force on the particles,  $\eta$  is the fluid viscosity,  $r_p$  is the radius of the nanobowl,  $v_f$  is the flow velocity and  $v_p$  is the particle velocity. It's clear that by increasing the viscosity of the fluid, radius of the nanobowls or the velocity difference between the flow and the nanobowls the drag force increases.

Note that as it was described before increasing the radius will increase the magnetic moment applied on the particles as  $F_m$  is directly proportional to  $r^3$  of the magnetic particles. If we assume that  $r_p$  is equal to  $r$  then the magnetic moment has a bigger affect on the nanobowls by 2 orders.

### 1.5 Velocity of the nanobowls

If we assume only the magnetic force and the drag force are the only two forces applied on the nanobowls that means ignoring the gravitational force and internal forces. Then using newtons third law the velocity of the nanobowls can be calculated as follows

$$-\mathbf{F}_{DP} = \mathbf{F}_m \quad \text{Eq(39)}$$

Substituting the magnetic force and the drag force in equation 39 we get the following.

$$-6\pi\eta r_p(\mathbf{v}_f - \mathbf{v}_p) = (\mathbf{m} \cdot \nabla)\mathbf{B} \quad \text{Eq(40)}$$

Rearranging equation 40 to find the velocity of the nanobowls

$$\mathbf{v}_f = \frac{(\mathbf{m} \cdot \nabla)\mathbf{B}}{6\pi\eta r_p} + \mathbf{v}_p \quad \text{Eq(41)}$$

Using this equation, the vector of the velocity of the nanobowls in the solvent can be found. This velocity can be then used to find the drag force applied on the nanobowls from equation 38. This helps in determining the ideal radius of the nanobowls based in the application and the viscosity of the fluid.

## CHAPTER 2

### **Experimental setup**

#### **2.1 Nanobowls protocol**

Magnetic nanobowls have been made in a step-by-step protocol [39]. 2 types of nanobowls have been made, one that has only the iron oxide ions which represents the magnetic part. And another one that has a lipid bilayer which can hold the Anle 138b drug. Both of these have a very similar protocol as described below

##### **2.1.1 Janus Template**

###### **2.1.1.1 Iron oxide and Anle 138b nanobowls**

Silica nanoparticles embedded with polystyrene were created by adding silica precursor and carboxylate polystyrene spheres to a buffer made out of water, alcohol and ammonium hydroxide. In a 20ml glass vial, 700ul of DI water, 4ml of Isopropanol (IPA) and 1.3ml of 28% ammonium hydroxide was added in order with a small stirring bar and set to stir on a magnetic plate. To the same glass vial while stirring, 55ul of Tetraethyl orthosilicate (TEOS) and 100um of carboxylate polystyrene spheres 2.7% in water (PS-COOH) of size 100nm was added at the same time and allowed to stir for 2 hours at room temperature. The solution gets whiter with stirring until a certain time about 1hour from the start of stirring due to the changing size of the nanobowls from the reaction happening between the TEOS and polystyrene spheres.

After stirring for 2 hours the solution, was removed into a centrifuging tube and spun at 500g for 5 minutes to remove the large size particles. The supernatant was then removed to another centrifuging tube and washed 3 times in 3ml of DI water by sonicating and centrifuging for 10 minutes each time. After washing is done, the pellet was then resuspended in 2ml of EtOH by vortexing and sonicating for 10 minutes.



This step will produce a negativity charged silica nanobowls with an opening that has polystyrene embedded inside. The size of all the nanobowls are very close and some aggregation has been produced.

## **2.1.2 measuring the yield of nanobowls**

### **2.1.2.1 Iron oxide and Anle 138b nanobowls**

It's critical to measure the yield of the nanobowls so that the concentration of nanobowls is correct which helps in reducing the aggregation. To measure the yield, the weight of a 20ml empty glass vial was measured without a cap. Then, the Janus template solution that was made before in the class vial was transferred and left it in a vacuum desiccator at 60-80 °C overnight or until the Ethanol is fully evaporated.

Once the Ethanol is fully evaporated, the nanobowls will be a powder at the bottom of the glass vial. The weight of the glass vial with the dried Janus template inside was measured and the difference was calculated between the 2 weights. the dried Janus template were resuspended in DI water with a ratio of 1.56mg/ml by sonicating for 20 minutes.

## **2.1.3 preparing lipid bilayer with drug inside**

### **2.2.3.1 Anle 138b nanobowls**

This step was only used for Anle 138b nanobowls. The lipid bilayer was made with the drug needed to be loaded. However different lipids with different drugs can be prepared by differentiating the ratios of the chemicals used. In a 20ml class vial add 924ul of 0.4mg/ml Anle 138b, 250ul of 10mg/ml 1,2-dioleoyl-sn-glycero-3-phosphoethanolamine (DOPE) and 417ul of 3mg/ml N-Isopropylacrylamide (NIPAM) were added. The solution was stirred on a stirring plate using a stir bar overnight. Once stirring is done, the lipid bilayer was dried using a rotovap or a vacuum desiccator overnight.

Since Anle 138b is very lipophilic, it will stay in the hydrophobic tail part of the lipid bilayer. This means that the Anle 138b drug will be fully encapsulated inside the lipid and ready to be attached to the Janus template.

## **2.1.4 Combining the nanobowls with the lipid bilayer**

### **2.1.4.1 Anle 138b nanobowls**

Since the nanobowls are now suspended in DI water as was described in 2.1.2. We needed to resuspend the dried lipid bilayer in water too. 5ml of DI water was added to the dried lipid bilayer and sonicated for 15 minutes. Once the lipid bilayer is fully dissolved in water, 750ul of the 1.56mg/ml nanobowls was added to the glass vial that contains the lipid bilayer and prob sonicate on ice for 1.5 hours. To ensure full encapsulation the glass vial was covered with foil and stirred overnight.

The reason for covering the glass vial with foil is because NIPAM is light sensitive and if it gets exposed to light for some time it becomes unstable and release the drug. After this step is done Anle 138b Janus templates are ready. Those Janus templates were used to test the release of drug under different temperatures and PH.

## **2.1.5 Attaching iron oxide to Janus template**

### **2.1.5.1 Iron oxide Janus template**

To make the Janus template magnetic, amine iron oxide was attached. In a small centrifuging tube add 500ul of the 1.56mg/ml nanobowls was added to 10ul of 15nm amine iron oxide. The solution was stirred for 20 minutes at room temperature. After stirring, the solution was centrifuged for 5 minutes at 3200g. This will result in a brown pellet at the bottom which has the Janus templates coated with iron oxide. The pellet was resuspended in 700ul DI water by

vortexing and sonicating for 20 minutes. This will result in a positively charged Janus templates coated with iron oxide.

It's important to keep track of the surface charge so that the iron oxide get attached properly to the nanobowls. Since Silica and carboxylate polystyrene spheres are negatively charged, we must use amine iron oxide which is positively charged to become attached to the nanobowls.

## **2.1.6 Etching out the polystyrene**

### **2.1.6.1 Iron oxide nanobowls**

The polystyrene was removed from the Janus template to create a payload loading domain. To remove the polystyrene from the nanobowls we need to use Dimethyl Formamide (DMF) which only dissolves the polystyrene. In a glass vial, the iron oxide nanobowls were suspended in 5ml DMF and stirred in silicone oil at 60 °C overnight. Once stirring was done, wash the nanobowls with ethanol 3 times by centrifuging at 3200g for 10 minutes.

After this step, the magnetic nanobowls will be ready for drug loading. The next couple of sections (3.1.7 – 3.1.9) are some modifications that have been done to our specific study to increase the attachment and stability of iron oxide on the nanobowls which makes it more responsive to an external magnetic field.

## **2.1.7 Coating nanobowls with AEAPTMS**

The process of coating nanobowls with silane such as N-[3-(Trimethoxysilyl)propyl]ethylenediamine (AEAPTMS) is quite complicated as it depends on a lot of factors such as temperature, mixing time, concentration, and solvent type [43]. However, there are two reasons for to coat the nanobowls with a silane layer. First, is to convert the surface charge of the silica nanobowls from negative to positive so that it's possible to attach negatively

charged particles such as gold. And the other reason is to have the  $N_2H$  compound which will be used later to preform a cross linkage with iron oxide. However, silane might not entirely cover the nanobowls surface and in that case the charge of the nanobowls might not be positive enough to attract negatively charge particles.

To coat nanobowls with AEAPTMS an excessive amount of 40ul AEAPTMS was added to 1ml of the dispersed nanobowls in water to ensure covering of the nanobowls. This was mixed using a thermos-mixer at 60 °C and 1200 rcf overnight.

### **2.1.8 Activating an attaching iron oxide.**

Making nanobowls more magnetic is necessary to be able to control them to targeted places. However, the procedure varies depending on if the nanobowls are coated with AEAPTMS or not, but the process is easy. If this step was needed for the study, we replace it with section 3.1.5 and continue with the rest of the process without any changes. This process makes the attachment between the iron oxide and the silica Janus template more stable by forming a covalent bond.

For only Janus template, we can use amine iron oxide to make the nanobowls magnetic. To do that a 16.7 ul of 50% glutaraldehyde was mixed with 100ul of water. The solution was vortexed and 50 ul of 15nm amine iron oxide was added. This solution was left to tumble for 3 hours. After the tumbling is finished a 320ul of Janus template in water with a concentration of 1.56mg/ml was added and the solution and tumbled over night. Once this process is done, particles were washed in 1 ml of DI water 3 times.

On the other hand, if the Janus template was coated with AEAPTMS, then carboxylate iron oxide was used. A 13 mg/ml concentration of 1-ethyl-3-(3-dimethylaminopropyl) carbodiimide (EDC) in DI water was prepared. A 100 ul of EDC in DI water was add to 160 ul

of carboxylate iron oxide. The solution was vortexed, and 2 ml of Janus template coated with AEAPTMS was added. Then another 200 ul of EDC in DI water was added. This solution was left to tumble for 2 hours. EDC was used here because it preforms a cross linkage with the  $N_2H$  from the AEAPTMS. Both of those procedures work very well. However, AEAPTMS with carboxylate iron oxide procedure was more stable and the results were more consistent, so most of the testing was done on this type of nanobowls.

### 2.1.9 Coating the nanobowls with PEG

Coating with Methoxy poly(ethylene glycol) Thiol (mPEG-SH) makes the nanobowls more stable and mobile so that they can hold the drug and deliver it to the diseased region. mPEG-SH is used a lot in nanoparticles application due to the surface changes it makes. This helps in reducing toxicity, resistance to protein adsorption and help with attaching gold since the structure has SH attached at the tip [40] [23] [33].

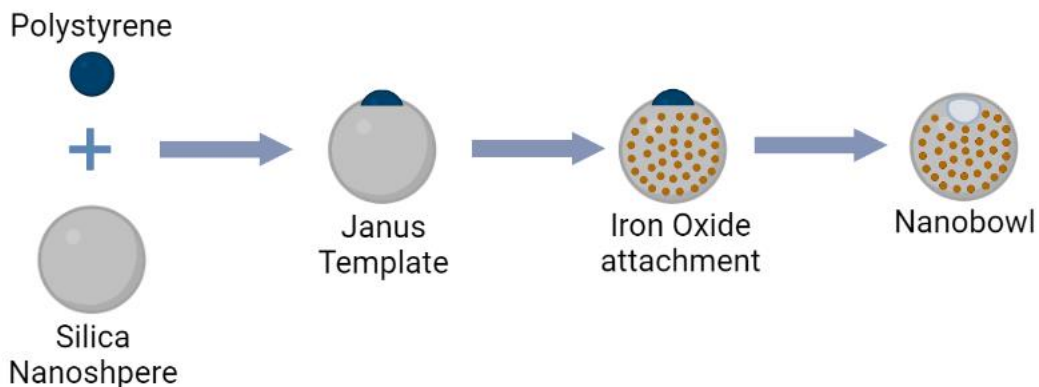


Figure 9: a non-detailed steps of having magnetic nanobowls

## 2.2 Microfluidic chip mold protocol

### 2.2.1 3D printing the mold

A 3D model was created with the appropriate dimensions on SolidWorks for the microfluidic chip using a ELEGOO Mars series SLA 3D printer with standard photopolymer resin to print the mold. Stereolithography (SLA) printers are considered one of the most accurate printers that produces a very smooth surface and has a dimensional tolerance of  $\pm 0.15\%$  and a lower limit of  $\pm 0.01$  mm [44].

After 3D printing is done, the mold was washed with IPA and water by adding IPA and water with a 1:1 ratio into a glass cub with the mold inside and sonicating for 3 minutes. Then the mold was washed again with only water and the surfaces wiped with IPA.

### **2.2.2 Treating the mold surface**

If Polydimethylsiloxane (PDMS) is used to create the microfluidic chip a treatment for the mold surface must be done, this is because PDMS gets stuck to the resin which prevent it from getting cured [47]. To solve this issue a treatment to the mold surface must be done.

Different resin types may need different treatment time however the procedure is still the same. Place the mold in a UV ozone machine for 1 hours, then heat the mold in oven for 6 hours at 120 °C. Now, the mold is ready to be used and the mold surface has been treated.

### **2.2.3 preparing the PDMS microfluidic chip**

PDMS was used to create the microfluidic chip because is cheap, not toxic and hydrophobic [47] [48]. Also, strong acid such as Hydrochloric acid (HCL) is used for cleaning the channels in the microfluidic chip, meaning the material of the chip should be a good resistance to both strong acid and strong base. Since PDMS is compatible with strong acids and bases then it should be a good choice for our chip [61]. To prepare the PDMS mix Sylgard 184 Silicone Elastomer Base with the curing agent with a 10:1 ratio and place it in a vacuum desiccator for 20 minutes to get rid of the bubbles. Pour the PDMS into the mold and vacuum it

again using a vacuum desiccator for another 20-30 minutes. Once the bubbles are all gone, place the mold with the PDMS inside a PDMS oven at 80 °C overnight or until the PDMS is fully cured.

Carefully remove the PDM from the mold and use the puncher to open the inlet and exit ports. To get the final usable product for the microfluidic chip, the PDMS needs to be attached to a glass slip so there is no overflow happening. Use Ultraviolet-Ozone with oxygen pressure and place the glass slip and the PDMS with the channel surface upward inside it for 10 minutes. Then place the PDMS on top of the glass slip with the channel surface on the glass and heat it up in a PDMS oven for 5-10 minutes at 80 °C [50].

## **2.3 Nanoparticles characterization**

### **2.3.1 SEM**

Scanning electron microscope (SEM) images were done on Zeiss Sigma 500. The sample was prepared by wrapping the stub with aluminum foil, then dropping around 10ul of the sample solution want to be tested and letting it dry. The images were taken at low voltage 2KV so that the sample doesn't burn.

The SEM was very useful to do after each step to ensure there was not as much aggregation and the nanoparticles exist with the right shape, size and surface roughness. SEM gives a clear image of the nanobowls with the holes and the iron oxide ions in 3D and measures their sizes. Also, through SEM the iron oxide nanoparticles per nanobowl can be counted by counting the number of iron oxide nanoparticles on one side and multiplying by 2.

### **2.3.2 TEM**

Transmission electron microscopy (TEM) images were captured on JEOL 1400 plus. The sample was prepared on a copper grid by dropping around 20ul of the sample solution want to test on parafilm paper and placing the grid shiny side down on the drop.

The TEM shows a 2D image of the nanobowls as well as the iron oxide nanoparticles and the cavities in the nanobowls. Using TEM is very important to see the nanobowls layers and how stable is the attachment is between the nanobowls and the iron oxide nanoparticles as well as measuring the cavities.

#### **2.3.4 EDS**

Energy dispersive X-ray spectroscopy (EDS) test was done on FEI Apreo SEM. The sample was prepared by dropping around 10-15 ul of the sample solution want to test on a double-sided tape on top of an SEM stub.

EDS gives the different concentration of a chosen compound in the sample at a specific point or area. This helps to determine the concentration of iron oxide and compare the activated and the non-activated samples.

#### **2.3.4 DLS**

Dynamic light scattering (DLS) tests were done on Zetasizer Nano ZS. There were two types of samples prepared on this machine zeta protentional which requires 800ul of the solution want to test and size which requires 100ul of the solution want to test. At each DLS test 3 trials have been done and 100 test for each trial.

The zeta potential test helps in determining the stability of the nanoparticles by giving the surface charge. This is very important to make sure you have the correct surface charge, and the iron oxide nanoparticles will be attached to the Janus template. The size test will give the size



distribution for the nanoparticles which helps in determining if there are any aggregations in the sample.

### **2.3.5 UV-Vis**

Ultraviolet–visible spectroscopy (UV-Vis) was done on a Tecan Infinite Pro Spectrometer. This machine can do many tests such as absorption and fluorescence. Sample was prepared by adding 100ul of the sample solution want to test into a grid well.

However, since Anle 138b becomes fluorescent when it is attached to  $\alpha$ -synuclein it was hard to test [51] [52]. On the other hand, Absorption test was very useful to determine if the solution has iron oxide nanoparticles in the controllability test.

### **2.3.6 High speed camera**

Optical microscope was used to capture the flow of the magnetic nanoparticles with solvent inside the microfluidic chip. The fluid was passed through into the microfluidic chip with a known flow using a syringe and a syringe pump. The syringe was connected to the microfluidic chip using a 0.04 inner diameter Tygon tubing.

On this microscope the frame rate can be controlled, although increasing the frames per second will decrease the time that can be recorded. A 1000 fps was used at a resolution of 1280x1024 and a magnification of x4.

## **2.4 Magnetic response**

As was mentioned before increasing the numbers of iron oxide particles attached to the nanobowls significantly increases the responsivity to a magnetic field. To test that we designed a system of microfluidic chip and used a magnet to attract the nanobowls to the magnet side of the chip channels.

### **2.4.1 Chip Reactor Microfluidic chip**

The type of microfluidic chip used here is a reactor, meaning that it has a rectangular cross section area. The microfluidic chip was prepared as was described in section 3.2 with a  $200 \times 200 \mu\text{m}$  cross section channel and a 1.2 mm diameter for the inlet and the outlets. The chip was attached to a glass slip using UV-ozone then cured in an oven for 5 minutes at  $80^\circ\text{C}$ .

Nanobowls suspended in a solvent were passed through the microfluidic chip using a 3ml syringe and an extreme-temperature Teflon PTFE semi-clear tubing for chemicals with an inner diameter of 0.03125 in and an outer diameter of 0.0625. The flow was controlled using a syringe pump. The channel in the microfluidic chip has a Y shape, a parent and 2 daughters as shown in the figure below.  $5/8" \times 5/8" \times 5/8$  magnet with a pulling force of 27.83 lbs was used to attract the nanobowls to one of the daughters' channels by having it 1 cm away from the bifurcation point and on the desired side to attract the nanobowls to. After the test is done a UV-Vis machine has been used to test the absorption of the solvent with the nanobowls on the magnetic side, nonmagnetic side and at the inlet. The test was done at 450nm wavelength which is in the range of the visible light wavelength and that is where the nanoparticles start to have a reasonable value. The absorbance test was done on a different concentration of the nanobowls, and the data was recorded and processed.



## CHAPTER 3

### Experimental results

#### 3.1 magnetic nanobowls synthesis

This section will explain the synthesis of AEAPTMS coated silica nanobowls with activated carboxylate iron oxide attached. This was the most stable, repeatable and reproduceable procedure.

##### 3.1.1 Silica nanospheres with polystyrene

Nanobowls were created in a layer-by-layer fashion. This was done to avoid aggregation by washing the particles multiple times during each layer and making them stable. First step was to create the silica nanosphere ( $\text{SiO}_2$ -NS) with a core made by polystyrene (PS) as shown in figure 11 below. The nucleation was done by polymerization of a silica precursor (TEOS) colliding with PS spheres and surrounding it.

The collision between TEOS and PS reduces the size of the silica spheres by making the TEOS to tightly cluster around the PS. From the images of the SEM and TEM we can observe that are some silica spheres have more than one PS attachment, where 30% has a single cavity, 40% with double cavities and 30% with more than 2 cavities [54]. Increasing the number of cavities increases the core volume which helps in loading more drug inside, however the more cavities make the nanobowls less stable. Also, The average size of the silica spheres with the PS it about 260nm. This size can be controlled by controlling the stirring time of the TEOS with the Polystyrene and the concentration of TEOS.

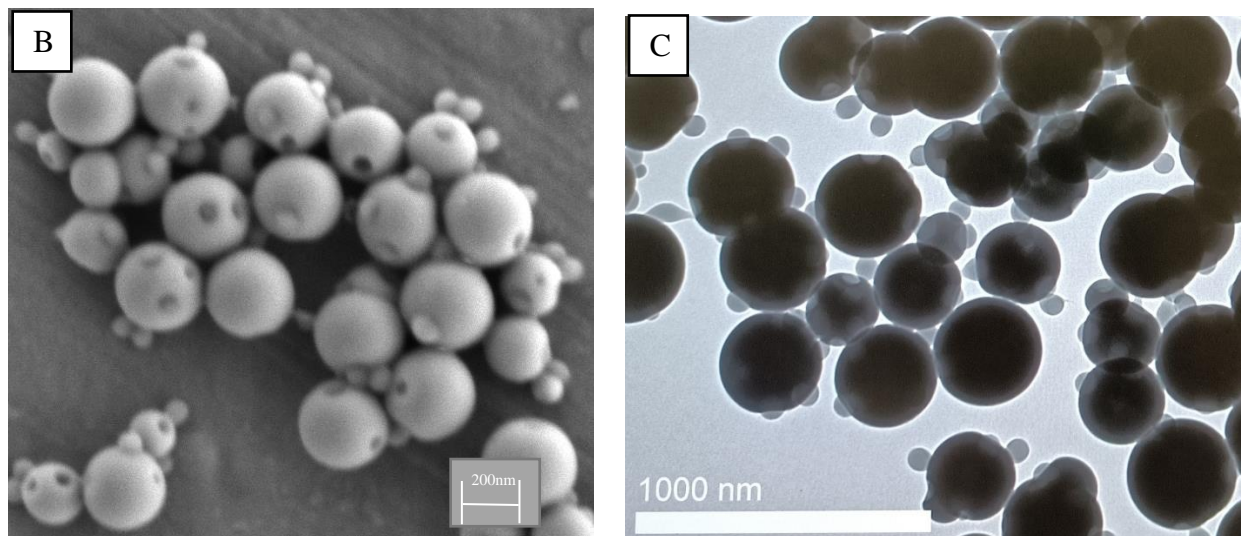
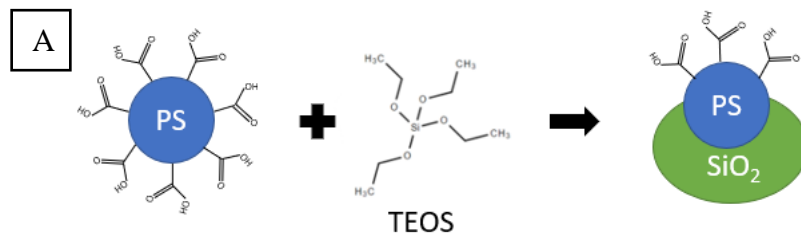


Figure 11: A) TEOS collides with polystyrene to form a silica nanoparticles with polystyrene inside. B) SEM image of silica spheres with polystyrene inside C) TEM image of silica spheres with polystyrene inside

### 3.1.2 Coating with silane

An amino silane was used to modify the surface of the silica sphere and to make it able to attach to carboxylate iron oxide. AEAPTMS ((3-Aminopropyl)triethoxysilane) was used for amino silane coating. AEAPTMS has a positive charge which makes the charge of the silica sphere to change from negative to slightly positive as it will be shown later.

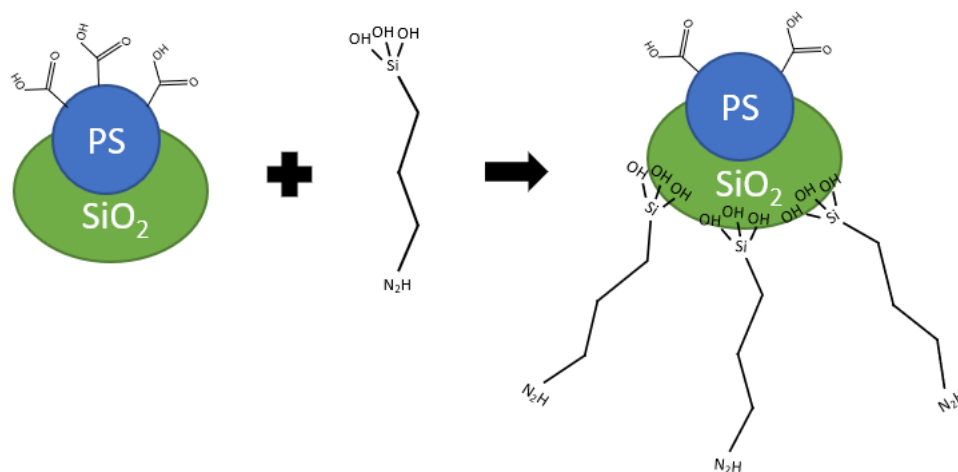


Figure 12: An amino silane ((3-Aminopropyl)triethoxysilane is attached to the silica sphere to modify the surface for carboxylate iron oxide attachment

To make sure that AEAPTMS cover most of the silica spheres an excessive of 40ul was added to a 1ml of Janus templates suspended in ethanol from step 4.1.1. This solution was used and left on stirring in a thermos-shaker at 60 °C and 1200 rpm overnight.

### 3.1.3 Iron oxide activation

Activating iron oxide is very critical to get a better attachment to the silica spheres. There are 2 types of carbodiimide compounds that can be used for carboxylic iron oxide activation which are 1-ethyl-3-(3-dimethylaminopropyl) carbodiimide hydrochloride (EDC) and N'-dicyclohexyl carbodiimide (DCC). In our case, since the silica spheres with PS coated with AEAPTMS are suspended in water, EDC was used. The reason for using EDC and not DCC is because EDC is water-soluble and used for aqueous crosslinking, whereas DCC is water-insoluble and used for non-aqueous organic synthesis [55].

To perform the activation, EDC was used and added to carboxylate iron oxide to form an O-acylisourea active ester. This will allow the iron oxide to form a cross linkage with the amino silane (AEAPTMS) that was used to coat the silica spheres. Pervious protocols have used

carboxylate iron oxide which has a negative charge and have directly added it to the coated silica spheres which has a positive charge from the AEAPTMS coating and allow it to react. This method doesn't form any linkages, and the carboxylate is attached to the silica spheres only because they have opposite charges. However, using this method shows to have a very unstable results and the iron oxide can be washed away easily. This will be described in more details later in this chapter with some SEM and TEM images.

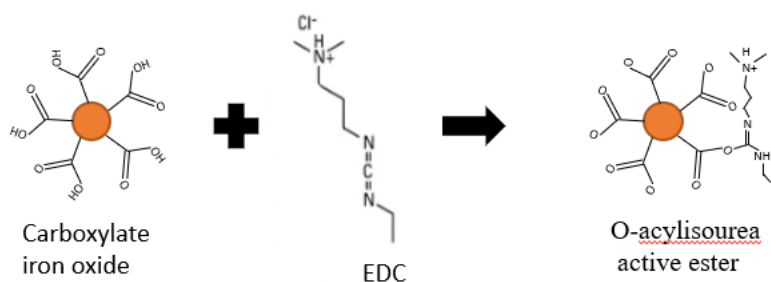


Figure 13: Activation of carboxylate iron oxide using EDC

### 3.1.4 Attaching iron oxide to silica spheres

After the carboxylate iron oxide is activated and the silica spheres with PS is coated with AEAPTMS, now they can be combined and mixed to perform a cross linkage attachment. While this is an easy process, it is not favorable to mix for more than 2 hours as EDC causes the particles to aggregate.

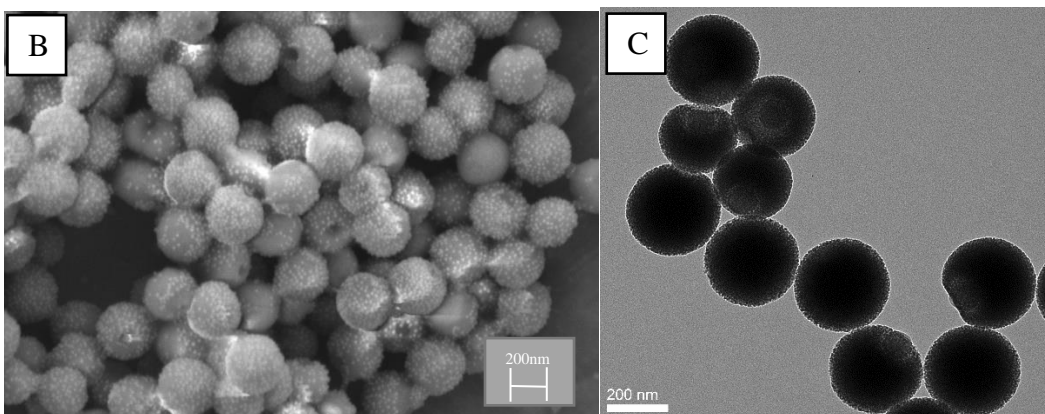
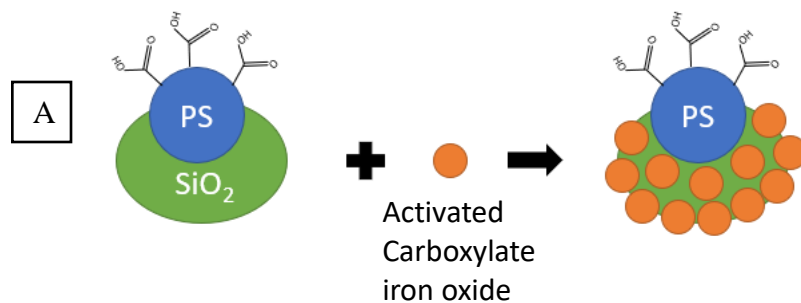


Figure 14: A) diagram shows attachment of carboxylate iron oxide to silica spheres with PS B) SEM image of attached iron oxide to silica spheres C) TEM image of attached iron oxide to silica spheres

It's important to note that diagram A does not show that actual number of iron oxide attachments. We can also see that most of the silica spheres here have only 1 hole, and iron oxide attachment is very concentrated and well distributed on the silica surface which make it very stable and responsive for a magnetic field.

### 3.1.5 Etching PS

As PS is soluble in DMF, stirring it under heat helps in removing the PS from the silica spheres and finally form nanobowls. After this step, nanobowls can be loaded with drug and coated a polymer such as silica or NIPAM to prevent any leakage.



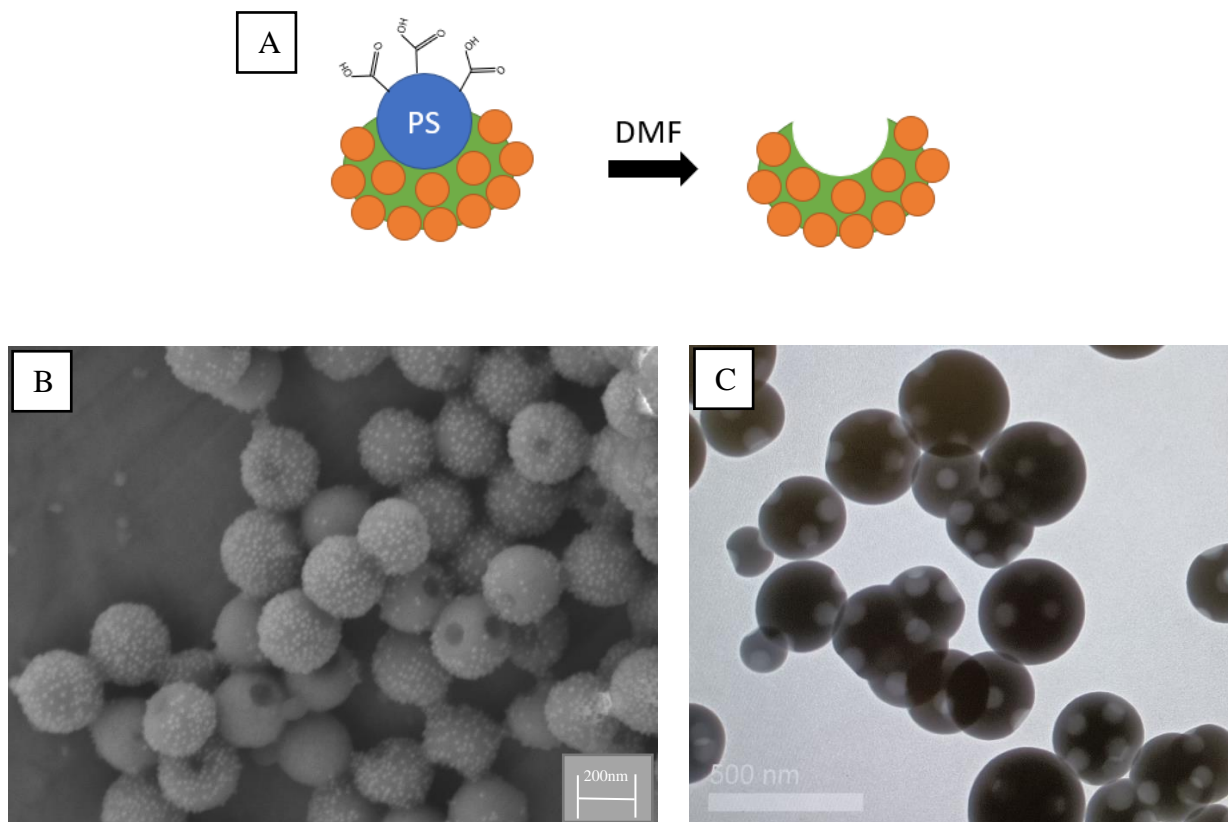


Figure 15: A) schematic shows the DMF dissolves only the PS form the silica nanospheres and produces nanobowls B) SEM image of nanobowls with carboxylate iron oxide C) TEM of nanobowls without iron oxide attached to better see the cavities

In the SEM image we note that some nanobowls has a very few iron oxide attachment which shows that still some of the iron oxide gets washed away. A TEM image was captured without iron oxide attached to better see the cavity. The depth of the cavity which was the distance from the silica surface to the bottom of the cavity was on average of 80 nm.

### 3.2 Characterization testing

#### 3.2.1 Comparing nanobowls with and without iron oxide activation

As was mentioned before, activation of iron oxide forms a better attachment with the silica spheres and make it more stable. The number of attachments was clearly increased in the SEM images. However, EDS also showed how the concentration is different. A test was done on 2 samples with activation and without activation.

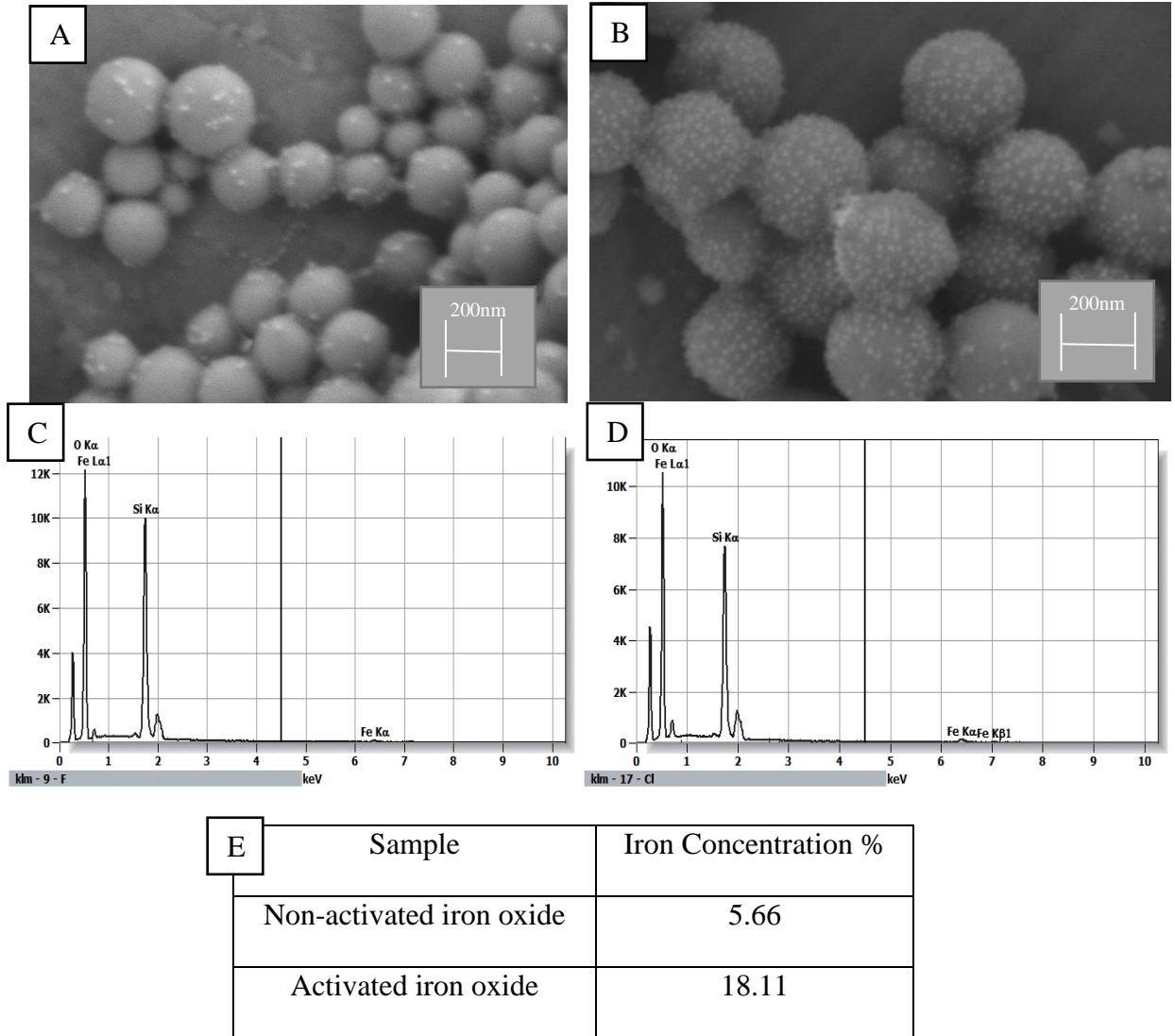


Figure 16: A) SEM image of silica nanospheres with non-activated iron oxide. B) SEM image of silica nanospheres with activated iron oxide. C) EDS data shows the compounds in non-activated iron oxide sample. D) EDS data shows the compounds in activated iron oxide sample. E) Iron concentration of each sample from the EDS data.

From the SEM images and the EDS data the concentration of iron has increased by almost 3 times in the activated iron oxide, meaning the number of the iron oxide particles attached to the silica spheres has increased. This increases the magnetic responsivity by a huge factor has was shown in figure 3.

On the other hand, even though the particles were made superparamagnetic, there is still a small magnetic force between the particles. This magnetic force increases by increasing the number of iron oxide attachment which leads to an aggregation. This means that the sample will not last for a long time and it was noted that after 2 weeks, the sample is fully aggregated and can not be used even if it was sonicated.

### 3.2.2 Surface charge

Using zeta potential on DLS allows us to determine the surface at each step of the synthesis. This helps in deciding what type of iron oxide to use (amine iron oxide or carboxylate iron oxide) and if there is any coating required before moving to the next step.

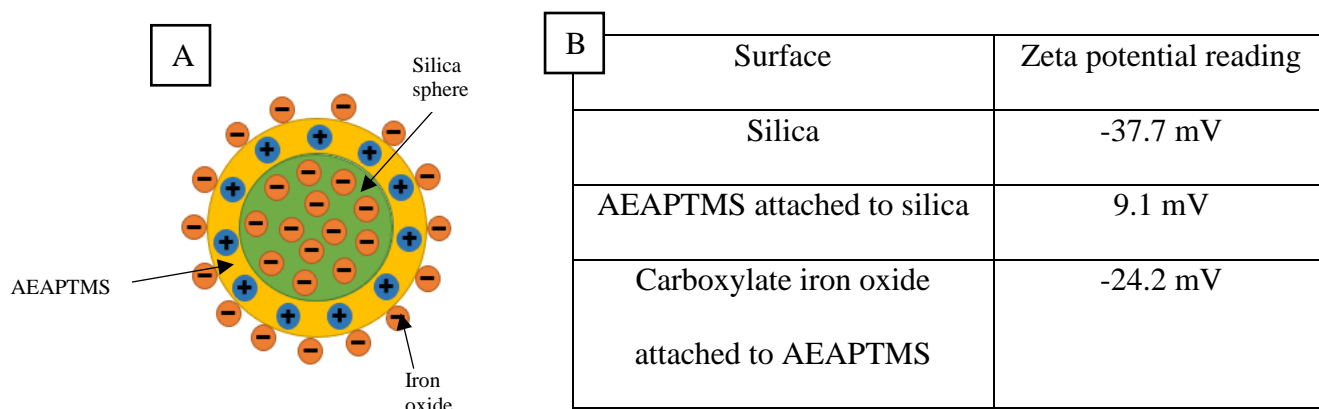


Figure 17: A) a schematic of the surface charge in green shows the silica sphere with negative charge coated with AEAPTMS positive charge and the carboxylate iron oxide with negative charge. B) The actual average reading of 5 different sample on zeta potential

From this data we can make 2 observations. First is that AEAPTMS changes the charge of the silica sphere from negative to positive. However, the surface charge still does not have a high positive charge. This is because of two factors, AEAPTMS doesn't cover the whole surface of the nanobowls and not all the nanobowls are coated with AEAPTMS. This results confirms that attaching iron oxide without activation and depending only on the charge will fail as it was described in 3.1.3.

The second observation is that by measuring the charge of the carboxylate iron oxide by itself it gives a value between -30 mV to -45 mV. But the charge of the nanobowls with carboxylate iron oxide has an average value of -24.2 mV meaning that carboxylate doesn't cover the entire surface of the nanobowl and there is still AEAPTMS exposed on the surface. Also, some nanobowls have a few attachments on carboxylate iron oxide as can be seen in figure 15 above.

### **3.2.2 Size**

The size of the nanobowls was measured using DLS and SEM. It was noticeable that after 2 weeks the particles start to aggregate which results in increase in the size measured by the DLS. Also, 2 weeks after attaching the iron oxide, there was a huge increase in the size due to the internal attractive force between the nanobowls.

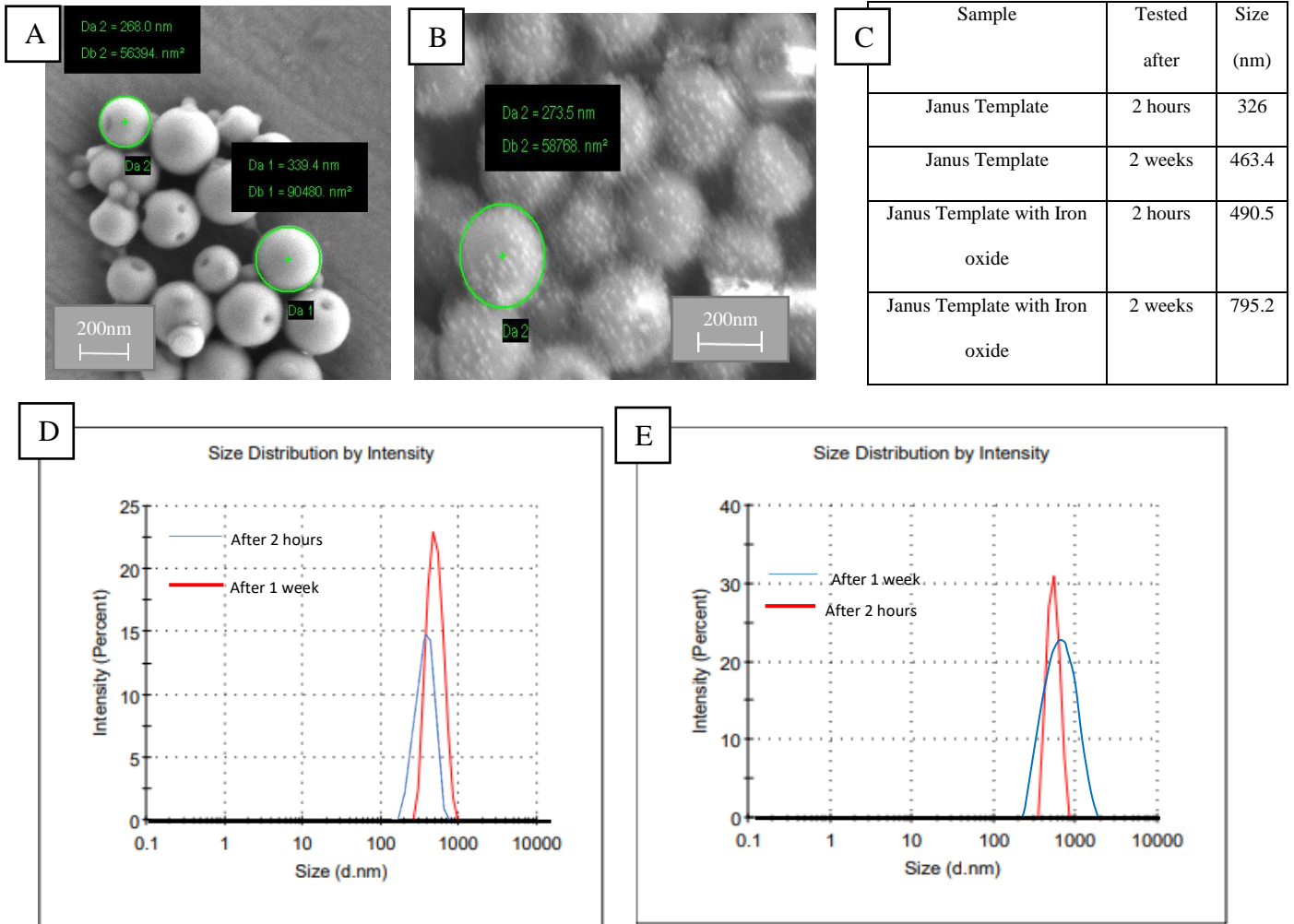


Figure 18: A&B) SEM image shows the size of the nanobowls C) Size distribution of nanobowls after 2 hours and 1 week D) size distribution of nanobowls without iron oxide E) size distribution of nanobowls with iron oxide

From the SEM images, we see that the individual sphere size for nanobowls with and without iron oxide is almost the same. However, from the DLS data the nanobowls with iron oxide clusters faster and starts to form big chunks. Whereas the nanobowls without iron oxide don't cluster as much as the ones with iron oxide. This is what is called aggregation and happens because of the internal force between the particles or because gravitational sedimentation is not high enough to overcome thermal energy. A possible solution to this is to filter the sample, but that might cause a loss in the nanobowls and as a result, reduces the concentration. Or by

sonicating, where it helps in evenly scattering the nanobowls but doesn't solve the aggregation issue completely.

Also, it's important to notice that the nanobowls here were not coated with any layer after the attachment of iron oxide which means the internal force is maximized and the aggregation is large. It's recommended to coat the nanobowls with polymer such as PEG or another silica layer depending on what the nanobowls are going to be used for. This polymer helps in mobility of the nanobowls inside the blood vessels and helps in making the nanobowls more stable and keeping the iron oxide protected. It also reduces the internal forces between the nanobowls.

### 3.2.4 Flow using high speed camera

A high-speed camera was set-up with a back lighting to check and confirm that the assumptions made in 1.3.1 hold. The flow was done using nanobowls with iron oxide attached, and a picture with videos were captured at different times and speeds.

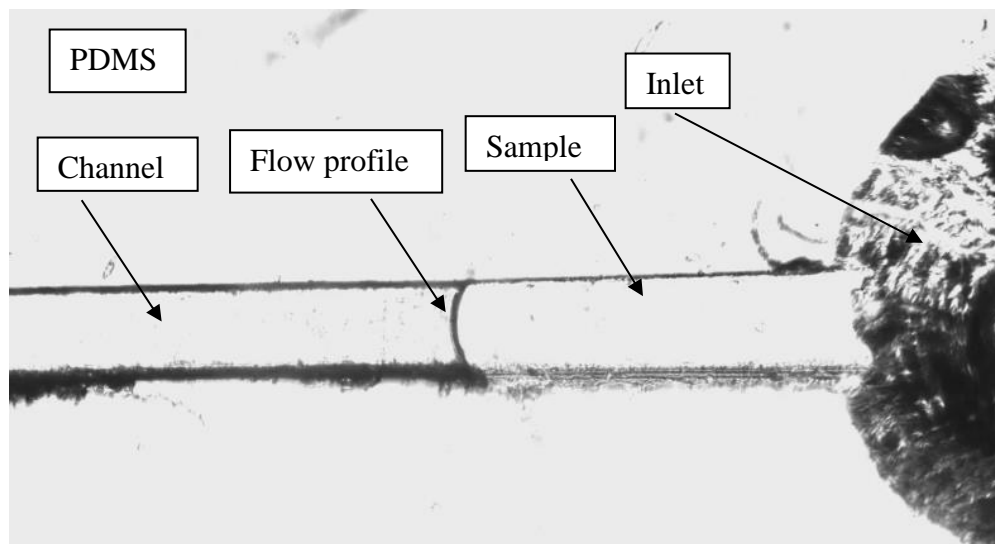


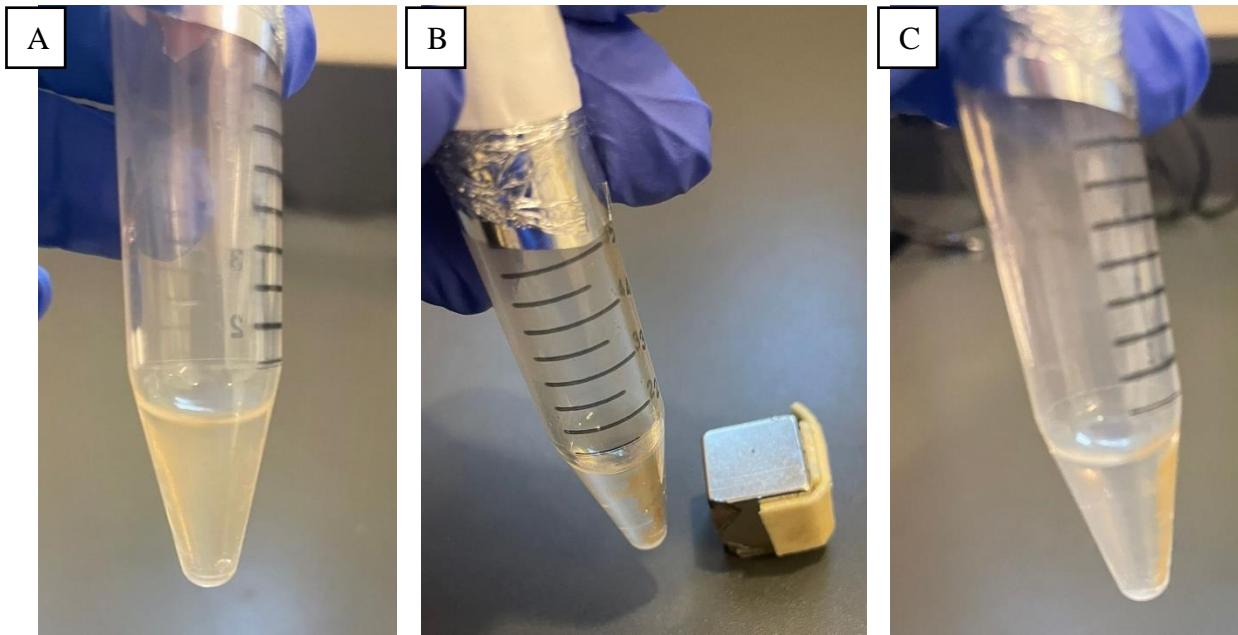
Figure 19: Flow profile inside a microfluidic channel

The flow had the same parabolic profile shown in figure 19 over the whole PDMS channel and at different flow rates. This shows that it's fully developed and has no slip boundary conditions.

### 3.3 Controllability

#### 3.3.1 Responsivity

The responsivity of the nanobowls to a magnetic field can be tested before using the system of the microfluidic chip. It is possible to test the responsivity simply by moving the magnet closer to the container of the nanobowls. This was done using different magnet sizes and forces. The distance at which the magnet starts attracting the nanobowls was reported as follows.



Magnet size	Pulling Force	Distance
Cube (3/16" x 3/16" x 3/16")	2.83 lbs	0.65 cm
Cube (1/2" x 1/2" x 1/2")	18.71 lbs	1.6 cm
Cube (5/8" x 5/8" x 5/8")	27.83 lbs	1.95 cm

Figure 20: A) magnetic nanobowls dispersed in water B) magnetic nanobowls getting attached using a 0.4T magnet with pulling force of 18.71 lbs. C) nanobowls moved to the magnet side D) shows the distance where the nanobowls start getting attracted after the presence of different magnet size and pulling force

All the three magnets are N42 with the same surface field and coated with nickel.

However, the size difference makes them have different pulling forces. As expected, increasing

the pulling force makes the magnet able to pull the magnetic nanobowls at a further distance which helps in solving some issues, but still cannot reach deep tissues which are 6-10cm away from the skin. For this reason a Halbach is used which consists of multiple magnets combined together in different shapes to provide the maximum pulling force.

### 3.3.2 Absorbance

As was mentioned before the absorbance test of the nanobowls with the solvent gives the concentration of the nanobowls. To test the absorbance, a UV-Vis was used. Through UV-Vis, the concentration is related to the absorbance in a linear proportional relationship using the following equation

$$A = \epsilon CL \quad \text{Eq(36)}$$

Where A is the absorbance,  $\epsilon$  is the sample-specific extinction coefficient, C is the concentration and L is the optical path length for where the light travels. Keeping the L and  $\epsilon$  constants and only changing the C then the absorbance only depends on the concentration and that's what was done in the experiment.

The test was done using 2 solvents water and 22% glycerin with 78% water to increase the viscosity to the whole blood viscosity. After the magnetic nanobowls are fully dispersed in the solvent the experiment of the microfluidic chip was performed as described before where the magnet is only to one side of the microfluidic chip to attract the nanobowls one of the daughter channels.



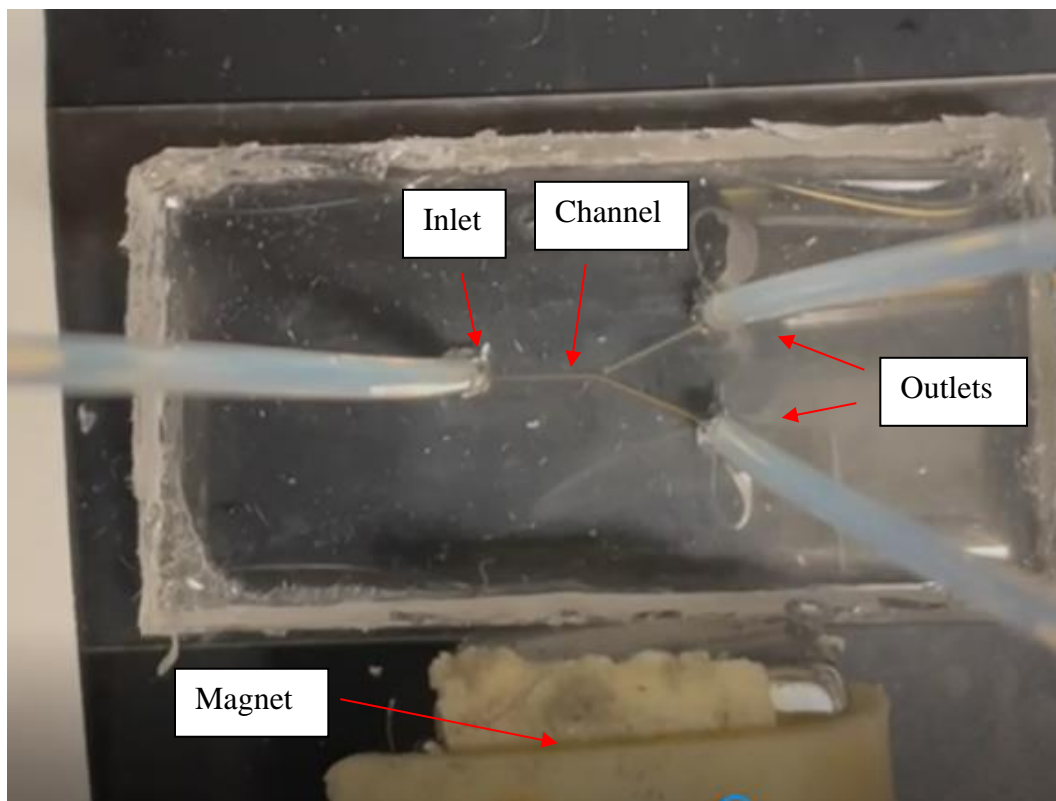


Figure 21: Nanobowls solvent is injected to the microfluidic chip with a magnet to one side

It is important to notice that by just looking at the flow the daughter channel from the magnet side has a browner color which indicates have more concentration of iron oxide nanobowls since the brown color comes from the iron oxide attached to the nanobowls. Then the absorbance test was performed at the inlet and both outlets.

### 3.3.2.1 Water Solvent

Water has a viscosity of  $1.002 \times 10^{-3} \text{ Ns/m}^2$ . The lower the viscosity, the easier for the nanobowls to move in the solvent which means it's easier to pull the nanobowls using a magnet. After passing the dissolved nanobowls through the microfluidic chip at 3 flowrates and testing the absorbance, we got the following results.

Table 1: Absorption of a reduced concentration of iron oxide nanobowls (IONBs) suspended in water at 3 different flow rates.

Concentration	(Magnet side, Inlet, Solvent)	Magnetization type	Absorbance at 2 ul/min	Absorbance at 10 ul/min	Absorbance at 20 ul/min
10 ul IONBs 90ul water	Inlet	Superparamagnetic	0.1227	0.1227	0.1165
10ul IO NBs 90ul water	Magnet side	Superparamagnetic	0.7414	0.5219	0.3056
10ul IO NBs 90ul water	Not magnet side	Superparamagnetic	0.0637	0.0956	0.1611
Water	N/A	N/A	0.059	0.059	0.059

From the table above, the absorbance of the solvent with iron oxide nanobowls on the magnet side is higher than the absorption of the sample at the inlet. This is because the concentration has increased by pulling the iron oxide nanobowls to one side of daughter channels whereas the solvent is still split between the 2 daughter channels. Also, the absorbance in the magnet side is ~11.64 times higher than the non-magnet side, which means we were successful in pulling the magnetic nanobowls to the desired side. Lastly, the non-magnet side has an absorbance that is slightly higher than the water by itself. This means that the non-magnet side still has just a very few numbers of the nanobowls.

It's also very important to notice that the concentration of magnetic nanobowls reduces in the magnet side with increasing the flow rate whereas it increases in the nonmagnet side. This because increasing the flow rate increases the velocity of the flow, and as a result it increases the drag force getting applied on the nanobowls. However, the concentration in the magnet side is still higher by a factor of 11.64 for 2ul/min, 5.46 for 10ul/min and 1.90 for 20ul/min. To solve this issue, more than one magnet is required to increase the magnetic moment and the magnetic force applied on the magnetic nanobowls.

To better compare the results at the 3 different flow rates they were further diluted to reduce concentration and the absorbance was tested at each concentration as shown below.

A	Number on plot	Concentration	Absorbance at 2ul/min	Absorbance at 10ul/min	Absorbance at 20ul/min
	1	10 ul IONBs 90ul water	0.7414	0.5219	0.3056
	2	5 ul IONBs 95ul water	0.3366	0.2546	0.1366
	3	2.5 ul IONBs 97.5ul water	0.1629	0.1287	0.0775
	4	1.6 ul IONBs 98.4ul water	0.1569	0.1169	0.0639
	5	1.125 ul IONBs 98.875ul water	0.1014	0.0714	0.0595
	6	1 ul IONBs 99ul water	0.0731	0.0531	N/A

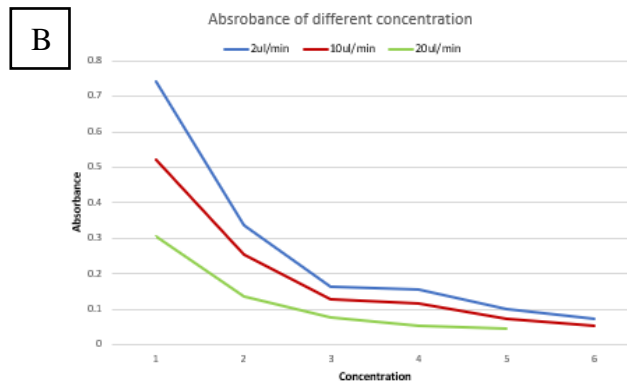


Figure 22: A) absorption measurement for different flowrates and concentration B) plot of absorption with concentration

For the flow rates 2ul/min and 10ul/min the same sample was used. There is a clear linear relationship between them. For 20ul/min a different sample was used however the curve still looks similar to that of the other 2 flow rates curves. This proves that the relation between absorbance and concentration described in equation 34 is correct. It also clearly shows the concentration of the magnetic nanobowls decreases by increasing the flow rate.

### 3.3.2.2 Glycerin-Water Solvent

As was described before, glycerin was added to the water to increase the viscosity to the whole blood viscosity between 3.5-5 cP. This makes it harder for the magnetic nanobowls to move in the solvent because of the increase in the drag force which will be represented in our results below.

Table 2: Absorption of a reduced concentration of iron oxide nanobowls (IONBs) suspended in glycerin-water at 3 different flow rates.

Concentration	(Magnet side, Inlet, Solvent)	Magnetization type	Absorbance at 2 ul/min	Absorbance at 10 ul/min	Absorbance at 20 ul/min
10 ul IONBs 90ul Glycerin-Water	Inlet	Superparamagnetic	0.1844	0.1844	0.1844
10ul IO NBs 90ul Glycerin-Water	Magnet side	Superparamagnetic	0.4437	0.2671	0.2007
10ul IO NBs 90ul Glycerin-Water	Not magnet side	Superparamagnetic	0.0435	0.1281	0.1611
Glycerin-Water	N/A	N/A	0.0397	0.0397	0.0397

As shown in the table, a similar result to what we got in the water solvent test was found. The concentration in the magnet side is still much higher than in the non-magnetic side and the sample inlet for the same reason that was described in the water solvent before. The nanobowls are attracted to the magnet side channel, but the solvent is split between the 2 daughters. Also, the non-magnet side absorbance is slightly higher than that of the solvent by itself which means it still has some magnetic nanobowls. On the other hand, note that by comparing the water solvent data to the glycerin-water solvent data we see that the sample concentration at the inlet here is higher. However, both outlets (with magnet and without magnet) have a lower concentration, as increasing the viscosity increases the shear stress as shown in equation 33. This

results in some of the magnetic nanobowls getting stuck at the wall of the PDMS and causing a reduction in the concentration. Another explanation to this is the absorbance constant of glycerin is smaller than that of water which means the absorbance of the glycerin will be less than water.

As was also described in the water solvent section increasing the flow rate decreases the concentration in the magnet side but increases it in the non-magnet side. But the concentration of the magnet side is still higher than the non-magnet side by a factor of 10.2 for 2ul/min, 2.08 for 10ul/min and 1.25 for 20ul/min.

A concentration comparison test was hard to perform here as the concentration for flow rates 10ul/min and 20ul/min was already low. And the solvent of glycerin-water is lower than that of only water which means diluting the magnetic nanobowls in more glycerin-water will reduce the concentration by a large factor.

### **3.3.3 Guiding efficiency on a larger scale of microfluidic chip**

Another microfluidic chip was created to have more bifurcations and an increased distance the distance between the bifurcation point and the magnet. In this test the flow rate used was 2ul/min and there was no absorbance measurements done, however the color of the solvent was sufficient to observe the guiding efficiency.

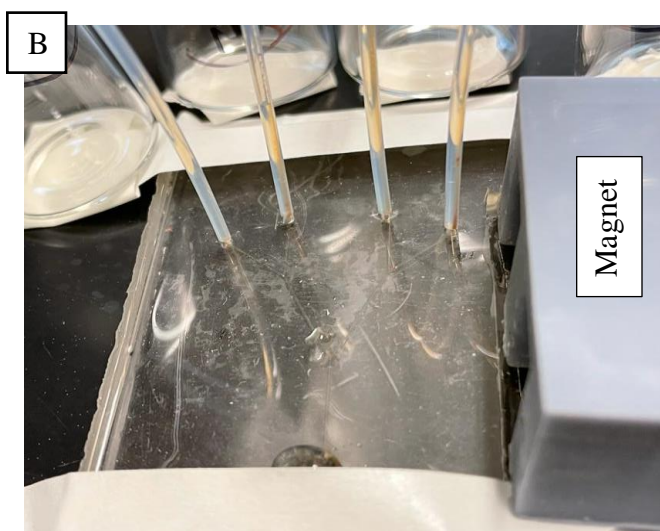
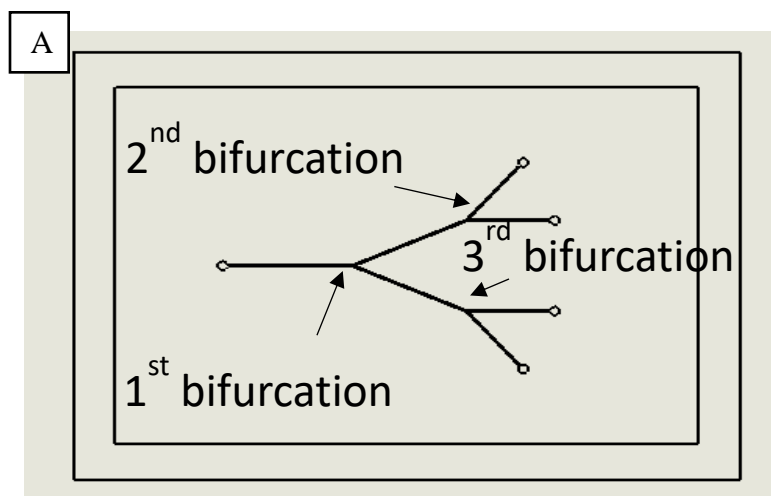


Figure 23 A) drawing of the microfluidic chip mold. B) nanobowls suspended in water passed through the microfluidic chip and collected at the four outlets. C) nanobowls suspended in glycerin-water passed through the microfluidic

The distance between the magnet and the bifurcation has been increased comparing to the microfluidic chip with only a single bifurcation. The magnet was placed 2.45cm from the first bifurcation point, 1.7cm from the second bifurcation and 2.9cm from the third bifurcation. For this test, 2 magnets were used and placed in a 3D printed fixture. Just by looking at the color of the solvent at the outlets, it was obvious that in water (image B) there was a successful attraction of the nanobowls. However, in glycerin-water (image C) there wasn't enough magnetic force to pull the magnetic nanobowls. This proves the point that was made before that increasing the

viscosity will increase the drag force on the particles, and as a result, reduce the ability of guiding those nanobowls to the desired location. The result also shows, the magnet was still able to attract the nanobowls suspended in water from a 2.45cm (first bifurcation) at low flow rate.

## CONCLUSION

### Work Done

This thesis covered how nanocarriers can help in targeted drug delivery by being able to control them using an external magnetic force. It also described a detailed synthesis of the magnetic nanocarriers that is made from silica and polystyrene to form a cavity for drug loading, as well as iron oxide to make it magnetic responsive. This is what we call magnetic nanobowls. An important observation that was made that increasing the amount of iron oxide attached increases the magnetization, but it also increases the internal force which cause them to aggregate and become unstable over time.

An important parameter in our magnetic nanobowls is the radius of the both the iron oxide and the nanobowls itself. Increasing the radius of our iron oxide attached on the nanobowls will increase its magnetization until it reaches the bulk size limit. It also increases the magnetic force being applied on the nanobowls as it was shown in equation 27, where the magnetic force is directly proportional to radius cubed of the iron oxide. On the other hand, to stay in the superparamagnetic regime, we have to stay in the range of 15 nm size of iron oxide or less for the room temperature case. The drag force on the nanobowls increases by increasing the size of the nanobowl itself where it was shown in equation 35 the drag force is directly proportional to the radius.

A controllability test was done on the magnetic nanobowls using a microfluidic chip to prove the ability of pulling them to the desired location. An absorbance test on the sample collected at the outlets and the inlet of the microfluidic chip showed that when the magnetic nanobowls were dispersed in water, the absorbance in the magnet side was 11.64 times higher than the nonmagnet side and 6.04 times higher than the inlet at 2ul/min flow rate. As the flow rate increases the absorbance in the magnet side starts to decrease and in the nonmagnet side



increases due to increasing the flow rate increases the velocity and as a result increases the drag force [60].

Lastly, using the same microfluidic system, another test was done using a more viscous solvent that was made from glycerin and water. Comparing it with water, a similar results were attained where the absorbance at the magnet side outlet is higher than that at the nonmagnet side and the inlet. In addition, by increasing the flow rate, the absorbance in the magnet side decreases whereas in the nonmagnet side increases. However, an important difference that the absorbance at the magnet side was 10.20 times higher than the nonmagnet side and 2.41 times higher than the inlet. This shows that by increasing the viscosity, the ability of pulling this magnetic nanobowls reduces due to the drag force and the shear stress increases this causes nanobowls to get stick to the microfluidic channel wall. Another explanation for this is that the sample specific extinction coefficient of the glycerin is less than water, which means glycerin has less absorbance than water.

### **Future Work**

It's important to keep in mind that the tests here were done in vitro. However, in vivo testing is required to experiment the effect of real blood and the blood vessels on the model as the blood and the vessels contains many components that can impact the pulling force applied by the magnet on the magnetic nanobowls.

The next step to improve targeted drug delivery through magnetic nanocarriers is to improve the magnetic force applied on by increasing the magnetic gradient. This can be accomplished by using an electromagnet, Halbach and doing multiple drag and magnetic force experiment on the radius of the magnetic nanoparticles, which was iron oxide in our study at different temperatures. Additional studies are required nanobowls to increase stability, load and

on-demand release of the drug, biocompatibility and degradability at different PH and organs of the body and the toxicity of increasing the iron oxide concentration.

## REFERENCES

- [1] C. Kaewsaneha, P. Tangboriboonrat, D. Polpanich, M. Eissa and A. Elaissari, *ACS Appl. Mater. Interfaces*, 2013, 5, 1857– 1869
- [2] Rizvi, Syed A A, and Ayman M Saleh. “Applications of Nanoparticle Systems in Drug Delivery Technology.” *Saudi Pharmaceutical Journal : SPJ : the Official Publication of the Saudi Pharmaceutical Society*, Elsevier, Jan. 2018, [https://www.ncbi.nlm.nih.gov/pmc/articles/PMC5783816/#:~:text=Due%20to%20their%20small%20size,skin%20\(Kohane%2C%202007\).](https://www.ncbi.nlm.nih.gov/pmc/articles/PMC5783816/#:~:text=Due%20to%20their%20small%20size,skin%20(Kohane%2C%202007).)
- [3] “Nanotechnologies.” 6. What Are Potential Harmful Effects of Nanoparticles?, [https://ec.europa.eu/health/scientific\\_committees/opinions\\_layman/en/nanotechnologies/1-3/6-health-effects-nanoparticles.htm#2p0](https://ec.europa.eu/health/scientific_committees/opinions_layman/en/nanotechnologies/1-3/6-health-effects-nanoparticles.htm#2p0).
- [4] Nguyen, Dung The, Nguyen, Vu, Tran and Ta. “On-Demand Release of Drug from Magnetic Nanoparticle-Loaded Alginate Beads.” *Journal of Analytical Methods in Chemistry*, Hindawi, 2 Apr. 2021, <https://www.hindawi.com/journals/jamc/2021/5576283/>.
- [5] Sant V, Som M, Karkisaval AG, Carnahan P, Lal R. Scavenging amyloid oligomers from neurons with silica nanobowls: Implications for amyloid diseases. *Biophys J*. 2021 Aug 17;120(16):3329-3340. doi: 10.1016/j.bpj.2021.07.002. Epub 2021 Jul 7. PMID: 34242592; PMCID: PMC8391079.
- [6] Wang, L., Jang, G., Ban, D. K., Sant, V., Seth, J., Kazmi, S., ... & Lal, R. (2017). Multifunctional stimuli responsive polymer-gated iron and gold-embedded silica nano golf balls: Nanoshuttles for targeted on-demand theranostics. *Bone research*, 5(1), 1-14.
- [7] Coveney, Reginald Davey Reviewed by Sophia. “Nanoparticles in Medicine.” *News*, 19 Apr. 2021.
- [8] Sun L, Chen X, Mu H, Xu Y, Chen R, Xia R, Xia L, Zhang S. Titanium Nanobowl-Based Nest-Like Nanofiber Structure Prepared at Room Temperature and Pressure Promotes Osseointegration of Beagle Implants. *Front Bioeng Biotechnol*. 2022 Feb 24;10:841591. doi: 10.3389/fbioe.2022.841591. PMID: 35284418; PMCID: PMC8908903.
- [9] Yin, Hong. “What Ketamine Actually Does to the Brain – New Frontiers Psychiatry & TMS: Milwaukee Psychiatrist.” *New Frontiers Psychiatry & TMS | Milwaukee Psychiatrist*, 8 Nov. 2021, <https://www.newfrontierspsychiatry.com/what-ketamine-actually-does-to-the-brain/>.
- [10] Deeg AA, Reiner AM, Schmidt F, Schueder F, Ryazanov S, Ruf VC, Giller K, Becker S, Leonov A, Griesinger C, Giese A, Zinth W. Anle138b and related compounds are aggregation specific fluorescence markers and reveal high affinity binding to  $\alpha$ -synuclein

- aggregates. *Biochim Biophys Acta*. 2015 Sep;1850(9):1884-90. doi: 10.1016/j.bbagen.2015.05.021. Epub 2015 May 29. PMID: 26028294.
- [11] Heras-Garvin A, Weckbecker D, Ryazanov S, Leonov A, Griesinger C, Giese A, Wenning GK, Stefanova N. Anle138b modulates  $\alpha$ -synuclein oligomerization and prevents motor decline and neurodegeneration in a mouse model of multiple system atrophy. *Mov Disord*. 2019 Feb;34(2):255-263. doi: 10.1002/mds.27562. Epub 2018 Nov 19. PMID: 30452793; PMCID: PMC6492169.
- [12] “Thermosensitive Gold Nanoparticles.” ACS Publications, <https://pubs.acs.org/doi/10.1021/ja038544z>.
- [13] Kono, K., Nakai, R., Morimoto, K., & Takagishi, T. (1999). Thermosensitive polymer-modified liposomes that release contents around physiological temperature. *Biochimica et Biophysica Acta (BBA)-Biomembranes*, 1416(1-2), 239-250.
- [14] “Chapter 6: Central Nervous System Infections.” AccessMedicine, <https://accessmedicine.mhmedical.com/content.aspx?bookid=2816&ionid=240347743>.
- [15] “Know Your Brain: Blood-Brain Barrier.” @Neurochallenged, <https://neuroscientificallychallenged.com/posts/know-your-brain-blood-brain-barrier>.
- [16] Bellettato, Cinzia M., and Maurizio Scarpa. “Possible Strategies to Cross the Blood–Brain Barrier - Italian Journal of Pediatrics.” BioMed Central, BioMed Central, 16 Nov. 2018, <https://ijponline.biomedcentral.com/articles/10.1186/s13052-018-0563-0>.
- [17] Gidwani, M. & Singh, A. V. Nanoparticle enabled drug delivery across the blood brain barrier: in vivo and in vitro models, opportunities and challenges. *Curr. Pharm. Biotechnol.* 14, 1201–12 (2014).
- [18] Hoshiar, A., Le, T.-A., Amin, F., Zhang, X., Kim, M. & Yoon, J. Noninvasive Guidance Scheme Delivery in Alzheimer ’ s Disease.
- [19] KnowledgeDose, and About KnowledgeDose. “Routes of Drug Administration.” KnowledgeDose, 2 Oct. 2020, <https://www.knowledgedose.com/routes-of-drug-administration/>.
- [20] Chomoucka, J., Drbohlavova, J., Huska, D., Adam, V., Kizek, R. & Hubalek, J. Magnetic nanoparticles and targeted drug delivering. *Pharmacol. Res.* 62, 144–149 (2010).
- [21] Kong, S. D., Lee, J., Ramachandran, S., Eliceiri, B. P., Shubayev, V. I., Lal, R. & Jin, S. Magnetic targeting of nanoparticles across the intact blood-brain barrier. *J. Control. Release* 164, 49–57 (2012).
- [22] McBain, Stuart C., Humphrey HP Yiu, and Jon Dobson. "Magnetic nanoparticles for gene and drug delivery." *International journal of nanomedicine* 3.2 (2008): 169.

- [23] WIREs Nanomed Nanobiotechnol 2015, 7:446–457. doi: 10.1002/wnan.1311
- [25] Thomsen, L. B., Thomsen, M. S. & Moos, T. Targeted drug delivery to the brain using magnetic nanoparticles. *Ther. Deliv.* 6, 1145–1155 (2015)
- [26] Kong, S. D., Zhang, W., Lee, J. H., Brammer, K., Lal, R., Karin, M. & Jin, S. Magnetically Vectored Nanocapsules for Tumor Penetration and Remotely Switchable On-Demand Drug Release. (2010). doi:10.1021/nl1033733
- [27] Mannell, H., Pircher, J., Räthel, T., Schilberg, K., Zimmermann, K., Pfeifer, A., Mykhaylyk, O., Gleich, B., Pohl, U. & Krötz, F. Targeted Endothelial Gene Delivery by Ultrasonic Destruction of Magnetic Microbubbles Carrying Lentiviral Vectors. *Pharm. Res.* 29, 1282–1294 (2012).
- [28] Iron Oxide Hazard Summary Iron Oxide - Government of New ...  
<https://nj.gov/health/eoh/rtkweb/documents/fs/1036.pdf>.
- [29] Khizar, S., Ben Halima, H., Ahmad, N. M., Zine, N., Errachid, A., & Elaissari, A. (2020). Magnetic nanoparticles in microfluidic and sensing: From transport to detection. *Electrophoresis*, 41(13-14), 1206-1224.
- [30] Lilia Romero, E., & Morilla, M. J. (2011). Topical and mucosal liposomes for vaccine delivery. *Wiley Interdisciplinary Reviews: Nanomedicine and Nanobiotechnology*, 3(4), 356-375.
- [31] Sarwar, A., Nemirovski, A., & Shapiro, B. (2012). Optimal Halbach permanent magnet designs for maximally pulling and pushing nanoparticles. *Journal of magnetism and magnetic materials*, 324(5), 742-754. [32] Studart AR, Amstad E, Gauckler LJ. Colloidal stabilization of nanoparticles in concentrated suspensions. *Langmuir*. 2007 Jan 30;23(3):1081-90. doi: 10.1021/la062042s. PMID: 17241017.
- [33] Kolhatkar, A. G., Jamison, A. C., Litvinov, D., Willson, R. C., & Lee, T. R. (2013). Tuning the magnetic properties of nanoparticles. *International journal of molecular sciences*, 14(8), 15977-16009.
- [34] Nayek, C., Manna, K., Imam, A. A., Alqasrawi, A. Y., & Obaidat, I. M. (2018, February). Size-dependent magnetic anisotropy of PEG coated Fe<sub>3</sub>O<sub>4</sub> nanoparticles; comparing two magnetization methods. In *IOP Conference Series: Materials Science and Engineering* (Vol. 305, No. 1, p. 012012). IOP Publishing.
- [35] Fannin, P. C., and S. W. Charles. "On the calculation of the Neel relaxation time in uniaxial single-domain ferromagnetic particles." *Journal of Physics D: Applied Physics* 27.2 (1994): 185.

- [36] Kötitz, R., Weitschies, W., Trahms, L., & Semmler, W. (1999). Investigation of Brownian and Néel relaxation in magnetic fluids. *Journal of magnetism and magnetic materials*, 201(1-3), 102-104.
- [37] Christopher, G.F.; Anna, S.L. Microfluidic methods for generating continuous droplet streams. *J. Phys. D. Appl. Phys.* 2007, 40, R319
- [38] Ward, K.; Fan, Z.H. Mixing in microfluidic devices and enhancement methods. *J. Micromech. Microeng.* 2015, 25, 94001.
- [39] Mo, A. H., Landon, P. B., Gomez, K. S., Kang, H., Lee, J., Zhang, C., ... & Lal, R. (2016). Magnetically-responsive silica–gold nanobowls for targeted delivery and SERS-based sensing. *Nanoscale*, 8(23), 11840-11850..
- [40] Larson, Timothy A., Pratixa P. Joshi, and Konstantin Sokolov. "Preventing protein adsorption and macrophage uptake of gold nanoparticles via a hydrophobic shield." *Acs Nano* 6.10 (2012): 9182-9190
- [41] Shon, Y.-S.; Mazzitelli, C.; Murray, R. W. Unsymmetrical Disulfides and Thiol Mixtures Produce Different Mixed Monolayer-Protected Gold Clusters. *Langmuir* 2001, 17, 7735–7741.
- [42] Eck, W.; Craig, G.; Sigdel, A.; Ritter, G.; Old, L. J.; Tang, L.; Brennan, M. F.; Allen, P. J.; Mason, M. D. Pegylated Gold Nanoparticles Conjugated to Monoclonal F19 Antibodies as Targeted Labeling Agents for Human Pancreatic Carcinoma Tissue. *ACS Nano* 2008, 2, 2263–2272
- [43] Mohapatra, S., Pramanik, N., Mukherjee, S., Ghosh, S. K., & Pramanik, P. (2007). A simple synthesis of amine-derivatised superparamagnetic iron oxide nanoparticles for bioapplications. *Journal of materials science*, 42(17), 7566-7574.
- [44] Nutma, Marinus. "A Quick Guide to Dimensional Accuracy for 3D Printing." *3D Printing Media Network - The Pulse of the AM Industry*, 4 Sept. 2019, [https://www.3dprintingmedia.network/quick-guide-dimensional-accuracy-3d-printing/#:~:text=Stereolithography%20\(SLA\)%20printing%20produces%20smooth,takes%20time%20to%20harden%20completely.](https://www.3dprintingmedia.network/quick-guide-dimensional-accuracy-3d-printing/#:~:text=Stereolithography%20(SLA)%20printing%20produces%20smooth,takes%20time%20to%20harden%20completely.)
- [45] Chen, H.; Burnett, J.; Zhang, F.; Zhang, J.; Paholak, H.; Sun, D. Highly crystallized iron oxide nanoparticles as effective and biodegradable mediators for photothermal cancer therapy. *J. Mater. Chem. B* 2014, 2, 757–765
- [46] Zaloga, J., Janko, C., Nowak, J., Matuszak, J., Knaup, S., Eberbeck, D. & Alexiou, C. (2014). Development of a lauric acid/albumin hybrid iron oxide nanoparticle system with improved biocompatibility. *International journal of nanomedicine*, 9, 4847.

- [47] Venzac, B., Deng, S., Mahmoud, Z., Lenferink, A., Costa, A., Bray, F. & Le Gac, S. (2021). PDMS curing inhibition on 3D-printed molds: why? Also, how to avoid it?. *Analytical chemistry*, 93(19), 7180-7187.
- [48] Friend, J., & Yeo, L. (2010). Fabrication of microfluidic devices using polydimethylsiloxane. *Biomicrofluidics*, 4(2), 026502.
- [49] Puthan, Pranav, et al. "Energetics and mixing in buoyancy-driven near-bottom stratified flow." *Journal of Fluid Mechanics* 869 (2019): 214-237.
- [50] Cargou, Sébastien. "Microfluidic Fabrication Technics." Elveflow, Elvesys, 14 Dec. 2020, <https://www.elveflow.com/microfluidic-reviews/soft-lithography-microfabrication/soft-lithography-fabrication-technics/>.
- [51] Deeg AA, Reiner AM, Schmidt F, Schueder F, Ryazanov S, Ruf VC, Giller K, Becker S, Leonov A, Griesinger C, Giese A, Zinth W. Anle138b and related compounds are aggregation specific fluorescence markers and reveal high affinity binding to  $\alpha$ -synuclein aggregates. *Biochim Biophys Acta*. 2015 Sep;1850(9):1884-90. doi: 10.1016/j.bbagen.2015.05.021. Epub 2015 May 29. PMID: 26028294.
- [52] Wagner, J., Ryazanov, S., Leonov, A., Levin, J., Shi, S., Schmidt, F.& Giese, A. (2013). Anle138b: a novel oligomer modulator for disease-modifying therapy of neurodegenerative diseases such as prion and Parkinson's disease. *Acta neuropathologica*, 125(6), 795-813.
- [53] James, M., Revia, R. A., Stephen, Z., & Zhang, M. (2020). Microfluidic synthesis of iron oxide nanoparticles. *Nanomaterials*, 10(11), 2113.
- [54] Lipid-encapsulated silica Nanobowls as an efficient and versatile DNA delivery system. (n.d.). <https://doi.org/10.1021/acs.bioconjchem.0c00493.s001>
- [55] Carbodiimide Crosslinker chemistry. Thermo Fisher Scientific - US. (n.d.). Retrieved June 16, 2022, from <https://www.thermofisher.com/us/en/home/life-science/protein-biology/protein-biology-learning-center/protein-biology-resource-library/pierce-protein-methods/carbodiimide-crosslinker-chemistry.html>
- [56] Pranav Suresh, S.S. Prasanna Kumar & B.S.V. Pantaik (2019) A Comparative Study of Two Different Density Estimation Techniques for Multi-Phase Flow Simulations Using SPH, *International Journal for Computational Methods in Engineering Science and Mechanics*, 20:1, 29-47, DOI: 10.1080/15502287.2018.1520756
- [57] Pranav Puthan, Masoud Jalali, Jose Luis Ortiz-Tarin, Karu Chongsiripinyo, Geno Pawlak, Sutanu Sarkar, The wake of a three-dimensional underwater obstacle: Effect of bottom boundary conditions

- [58] Puthan, Pranav, Geno Pawlak, and Sutanu Sarkar. "High Drag States in Tidally Modulated Stratified Wakes". *Journal of Physical Oceanography* 52.6 (2022): 1033-1048. <<https://doi.org/10.1175/JPO-D-21-0178.1>>. Web. 21 Jun. 2022.
- [59] Bellettato, C.M., Scarpa, M. Possible strategies to cross the blood–brain barrier. *Ital J Pediatr* 44, 131 (2018). <https://doi.org/10.1186/s13052-018-0563-0>
- [60] Puthan, Pranav, Sutanu Sarkar, and Geno Pawlak. "Tidal synchronization of lee vortices in geophysical wakes." *Geophysical Research Letters* 48.4 (2021): e2020GL090905.
- [61] "Solvent Compatibility of Poly(Dimethylsiloxane)-Based Microfluidic Devices." *Soft*, [http://soft-matter.seas.harvard.edu/index.php/Solvent\\_Compatibility\\_of\\_Poly\(dimethylsiloxane\)-Based\\_Microfluidic\\_Devices#:~:text=Influence%20of%20Swelling%20on%20PDMS,with%20most%20acids%20and%20bases](http://soft-matter.seas.harvard.edu/index.php/Solvent_Compatibility_of_Poly(dimethylsiloxane)-Based_Microfluidic_Devices#:~:text=Influence%20of%20Swelling%20on%20PDMS,with%20most%20acids%20and%20bases).
- [62] Delplace, Franck. "Laminar flow of Newtonian liquids in ducts of rectangular cross-section a model for both physics and mathematics." *Open Access Journal of Mathematical and Theoretical Physics* (2018): n. pag.